
iCITRIS: Causal Representation Learning for Instantaneous Temporal Effects

Phillip Lippe
QUVA Lab
University of Amsterdam
p.lippe@uva.nl

Sara Magliacane
MIT-IBM Watson AI Lab
University of Amsterdam

Sindy Löwe
UvA-Bosch Delta Lab
University of Amsterdam

Yuki M. Asano
QUVA Lab
University of Amsterdam

Taco Cohen
Qualcomm AI Research*
Amsterdam

Efstathios Gavves
QUVA Lab
University of Amsterdam

Abstract

Causal representation learning is the task of identifying the underlying causal variables and their relations from high-dimensional observations, such as images. Recent work has shown that one can reconstruct the causal variables from temporal sequences of observations under the assumption that there are no instantaneous causal relations between them. In practical applications, however, our measurement or frame rate might be slower than many of the causal effects. This effectively creates “instantaneous” effects and invalidates previous identifiability results. To address this issue, we propose iCITRIS, a causal representation learning method that can handle instantaneous effects in temporal sequences when given perfect interventions with known intervention targets. iCITRIS identifies the causal factors from temporal observations, while simultaneously using a differentiable causal discovery method to learn their causal graph. In experiments on three video datasets, iCITRIS accurately identifies the causal factors and their causal graph.

1 Introduction

Recently, there has been a growing interest in *causal representation learning* (Brehmer et al., 2022; Locatello et al., 2020a; Schölkopf et al., 2021; Yang et al., 2021), which aims at learning representations of causal factors in an underlying system from high-dimensional observations like images. Several works have considered identifying causal factors from time series data, assuming that the variables are independent of each other conditioned on the previous time step (Gresele et al., 2021; Khemakhem et al., 2020a; Lachapelle et al., 2022; Lippe et al., 2022b; Yao et al., 2022). This scenario assumes that within each discrete, measured time step, intervening on one causal factor does not affect any other instantaneously. However, in real-world systems, this assumption is often violated, as there might be causal effects that act faster than the measurement or frame rate. For instance, consider the example of a light switch and a light bulb. When flipping the switch, there is an almost immediate effect on the light by turning it on or off. In this case, an intervention on a variable (e.g. the switch) also affects other variables (e.g. the bulb) in the same time step, violating the assumption that each variable is independent of the others in the same time step, conditioned on the previous time step.

To overcome this limitation, we consider the task of identifying causal variables and their causal graphs from temporal sequences, even in the case of potentially instantaneous cause-effect relations. This task contains two main challenges: disentangling the causal factors from observations, and learning

*Qualcomm AI Research is an initiative of Qualcomm Technologies, Inc.

the causal relations between those factors. As opposed to temporal sequences without instantaneous effects, neither of these two tasks can be completed without the other: without knowing the variables, we cannot identify the graph; but without knowing the graph, we cannot disentangle the causal variables since they are not conditionally independent. In particular, in contrast to causal relations across time steps, the orientations of instantaneous edges are not determined by the temporal ordering, hence requiring to jointly solve the task of causal representation learning and causal discovery.

As a first step, we show that in the presence of potential instantaneous causal effects, we cannot identify the causal factors from observations, unless we have access to perfect interventions or strong additional assumptions. Intuitively, if the graph remains unchanged in all experiments, one cannot distinguish between entanglements in the observational space (*e.g.* images) and instantaneous causal relations. For example, consider a blue object illuminated by a white spotlight. If we change the spotlight color to red, the object will appear black. From purely observational data, we cannot distinguish whether the spotlight’s color caused a change in the object’s actual color, or if it just changed its appearance. However, if after performing a perfect intervention on the object color, *e.g.* by fixing it to green, we observe that the perceived object color is not the one we expected, then we can deduce how the entanglement happens in the observation function.

Further, we consider the general setting in which causal factors can be multidimensional. Following Lippe et al. (2022b), we focus on the *minimal causal variables*, *i.e.* the parts of the causal factors that are affected by the interventions, since interventions may leave some dimensions unchanged. In this setting, we prove that we can identify the minimal causal variables and their graph despite potentially instantaneous effects, if we have sequences with perfect interventions on known targets.

As a practical implementation, we propose *instantaneous CITRIS*, or *iCITRIS*, which, inspired by the recent causal representation learning method CITRIS (Lippe et al., 2022b), can discover the minimal causal variables and their causal graph for both instantaneous and temporal effects. *iCITRIS* maps high-dimensional observations like images to a latent space, on which it learns an instantaneous causal graph by integrating a causal discovery method into its prior. In particular, we consider two recent differentiable causal discovery methods: NOTEARS (Zheng et al., 2018) and ENCO (Lippe et al., 2022a). In experiments on three different video datasets, we show that *iCITRIS* can disentangle the causal variables while accurately recovering their causal graph. Overall, our contributions are:

- We show that one cannot identify causal factors in temporal sequences with instantaneous effects without perfect interventions or without additional assumptions.
- We prove that with perfect interventions with known targets, the minimal causal variables can be identified along with their causal graph from temporal sequences under mild assumptions.
- We propose *iCITRIS*, a causal representation learning method that identifies causal variables and their causal graph even in the case of potentially instantaneous causal effects.

2 Related Work

Most works in the field of causal representation learning have focused so far on identifying independent factors of variations from data (Klindt et al., 2021; Kumar et al., 2018; Locatello et al., 2019, 2020a,b; Träuble et al., 2021). As one of the first lines of work for this task, Independent Component Analysis (ICA) (Comon, 1994; Hyvärinen et al., 2001) tries to recover independent latent variables that were transformed by some invertible transformation. ICA was recently extended to non-linear transformations by exploiting auxiliary variables that make latents mutually conditionally independent (Hyvärinen and Morioka, 2016; Hyvärinen et al., 2019), and combined with deep learning methods like VAEs (Khemakhem et al., 2020a,b; Sorrenson et al., 2020; Zimmermann et al., 2021). Further, recent works draw a connection between causality and ICA (Gresele et al., 2021; Monti et al., 2019). In particular, Lachapelle et al. (2022); Yao et al. (2022) discuss identifiability of causal variables from temporal sequences. As forms of interventions, Lachapelle et al. (2022) consider external actions, while Yao et al. (2022) use non-stationary noise to model soft interventions. Yet, in all of these setups, all causal variables are required to be conditionally independent and scalar.

Focusing on causal structures in the data, von Kügelgen et al. (2021) demonstrate that common contrastive learning methods can block-identify causal variables that remain unchanged under augmentations. CITRIS (Lippe et al., 2022b) uses temporal sequences of observations with interventions to identify the minimal causal variables, *i.e.* the part of a potentially multidimensional causal variable

that is influenced by the provided interventions. Still, similar to works on ICA, CITRIS requires the causal variables within a time step to be independent conditioned on the previous time step, an assumption that is violated by instantaneous causal effects. Locatello et al. (2020a) identify independent latent causal factors from pairs of observations that only differ in a subset of causal factors. Brehmer et al. (2022) have recently extended this setup to variables with instantaneous causal effects. However, in contrast to our approach, Brehmer et al. (2022) require counterfactual observations where for a pair of observations, the noise term for all variables is identical, except for a single intervened variable. To the best of our knowledge, iCITRIS is the first method to identify causal variables and their causal graph from temporal, intervened sequences in the case of potentially instantaneous causal effects.

3 Identifiability in Temporal Intervened Sequences with Instantaneous Effects

We first describe our setting, Instantaneous TempoRal Intervened Sequences (iTRIS). We then discuss the challenges that arise due to instantaneous effects, and their implications on the identifiability of the causal factors. Finally, we present the identifiability results in iTRIS.

3.1 Instantaneous TempoRal Intervened Sequences (iTRIS)

iTRIS considers a latent temporal causal process with K causal factors $(C_1^t, C_2^t, \dots, C_K^t)_{t=1}^T$ with both causal relations across time steps, *i.e.* temporal, and within a time step, *i.e.* instantaneous. Instead of observing the causal factors directly, we measure a high-dimensional observation X^t from this process, representing a noisy, entangled view of all causal factors $C^t = (C_1^t, C_2^t, \dots, C_K^t)$ at time step t . The following paragraphs describe this setup in more detail, which is visualized in Figure 1.

Causal factors: We consider causal factors to be potentially multidimensional, *i.e.*, $C_i \in \mathcal{D}_i^{M_i}$ with $M_i \geq 1$ and the domain \mathcal{D}_i , for example \mathbb{R} for continuous variables. We define the causal factor space as $\mathcal{C} = \mathcal{D}_1^{M_1} \times \mathcal{D}_2^{M_2} \times \dots \times \mathcal{D}_K^{M_K}$.

Causal structure assumptions: We assume that the underlying latent causal process is a dynamic Bayesian network (DBN) (Dean and Kanazawa, 1989; Murphy, 2002) over the multi-dimensional random variables (C_1, C_2, \dots, C_K) that is first-order Markov, stationary, and potentially has instantaneous effects between different variables. This means that each causal factor C_i is instantiated at each time step t , denoted by C_i^t , and its causal parents $\text{pa}(C_i^t)$ can be any subset of the causal factors at time $t-1$ and t , including its own previous value C_i^{t-1} . Additionally, we assume that the complete structure of the graph is acyclic. Furthermore, the graph and its parameters are assumed to be time-invariant (*i.e.*, they repeat across each time step). Finally, we assume that the causal factors are causally sufficient (*i.e.*, there are no additional latent confounders) and that the distribution satisfies the causal faithfulness assumption (*i.e.*, there are no additional independences w.r.t. the ones encoded in the graph). Further details on the causal assumptions are in Appendix C.1.

Interventions: In each time step, we consider that interventions may have been performed on a subset of causal factors. We assume that we have access to the corresponding intervention targets, but not the sampled values of the intervened variables. We denote these targets by the binary vector $I^{t+1} \in \{0, 1\}^K$ where $I_i^{t+1} = 1$ refers to an intervention that has been performed on the causal variable C_i^{t+1} . Further, we assume the observational and interventional distributions to share the same

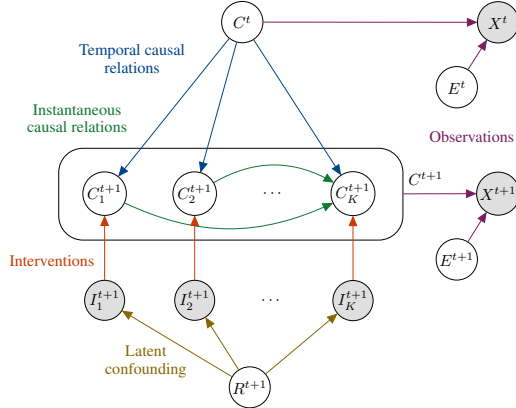


Figure 1: An example causal graph in iTRIS. A latent causal factor C_i^{t+1} can have as potential parents the causal factors at the **previous time step** $C^t = (C_1^t, \dots, C_K^t)$, **instantaneous parents** $C_j^{t+1}, i \neq j$, and its **intervention target** I_i^{t+1} . All causal variables C^{t+1} and the noise E^{t+1} cause the **observation** X^{t+1} . R^{t+1} is a potential **latent confounder** between the intervention targets.

support on \mathcal{C} . Finally, the intervention targets may be confounded by a latent regime variable R^{t+1} .

Observation function: We define the observation function $h(C_1^t, C_2^t, \dots, C_K^t, E^t) = X^t$, where E^t is any noise affecting the observation X^t independent of the causal factors C^t , and $h : \mathcal{C} \times \mathcal{E} \rightarrow \mathcal{X}$ is a function from the causal factor space \mathcal{C} and the space of the noise variables \mathcal{E} to the observation space \mathcal{X} . We assume that h is bijective, so we can identify each causal factor uniquely from observations.

3.2 Challenges in identifying causal variables with instantaneous effects

In iTRIS, causal variables within a time step can be related in two ways: they can be entangled by the observation function h to create the observation X^t , or they are causally related in the instantaneous causal graph, as discussed in the motivating example with a spotlight and an object changing colors in the introduction. To truly disentangle and identify the causal variables, we need to distinguish between these two forms of entanglement. Intuitively, a perfect intervention on a variable removes all its incoming edges, including instantaneous effects, thus excluding one type of entanglement.

To formalize this intuition, we consider an example in iTRIS with only two latent causal factors C_1 and C_2 , and, for simplicity, without temporal relations. We assume C_1 and C_2 do not cause each other, and the observation function is simply $X = [C_1, C_1 + C_2]$. We show that one cannot identify the causal factors or their graph from $p(X)$, since there are multiple different representations that can model $p(X)$ equally well. For instance, an alternative representation is $\hat{C}_1 = X_1 = C_1$, $\hat{C}_2 = X_2 = C_1 + C_2$ with the causal graph $\hat{C}_1 \rightarrow \hat{C}_2$, since $p(\hat{C}_2|\hat{C}_1) = p(C_1 + C_2|C_1) = p(C_2)$ and hence $p(\hat{C}_1, \hat{C}_2) = p(C_1, C_2) = p(X)$. Even under soft interventions that change the conditional distributions of C_1 and C_2 , we cannot necessarily tell the two representations apart, because the causal graph can remain unchanged under soft interventions.

Perfect interventions, on the other hand, force the intervened variable to be independent of its parents, which includes instantaneous effects. Thus, under perfect interventions on C_2 , the identified representation of C_2 must be independent of all its parents, including any potential instantaneous effect. This eliminates the possible representation of $\hat{C}_2 = C_1 + C_2$, since $C_1 + C_2 \not\perp C_1|I_2 = 1$ implies $\hat{C}_2 \not\perp \hat{C}_1|I_2 = 1$. Thus, we come to the following conclusion:

Lemma 3.1. *A causal variable C_i cannot always be uniquely identified in iTRIS if C_i potentially has instantaneous parents and the available data does not contain any perfect intervention on C_i .*

We provide the proof for this lemma and an example with temporal relations in Appendix C.2.1. From this lemma, it also follows that if we do not have perfect interventions on a causal variable C_i , we can only disentangle it from a set of other causal variables, $\tilde{\mathcal{C}}$ where $C_i \notin \tilde{\mathcal{C}}$, if we assume that C_i does not have instantaneous parents in $\tilde{\mathcal{C}}$. Otherwise, there may exist additional representations, similar to the example before, where C_i is entangled with other causal variables in $\tilde{\mathcal{C}}$.

3.3 Identifying the minimal causal variables

As a result of Lemma 3.1, we extend our assumptions to identify the causal variables. First, we assume that all interventions performed are perfect, *i.e.* $p(C_i^t|\text{pa}(C_i^t), I_i^t = 1) = p(C_i^t|I_i^t = 1)$. We require that the causal variables on which interventions are never performed in the observed sequence, *i.e.* $\forall t, I_i^t = 0$, are not instantaneous children of any variable with observed interventions. Further, to differentiate between interventions on different variables, we assume that no intervention target is a deterministic function of any other, *e.g.* by not allowing $\forall t, I_i^t = I_j^t, i \neq j$. Finally, if there exist symmetries in the distribution of a causal variable C_i , the representation of C_i may depend on other causal variables without changing the likelihood. For instance, a one dimensional Gaussian has the symmetry of flipping the variable C_i around its mean. Thus, C_i could be flipped, conditioned on another variable $C_j, i \neq j$, without changing the likelihood. To break this symmetry, the mean must depend on the intervention target and/or any variable from the previous time step. Hence, we assume that the temporal dependencies and provided interventions break all symmetries in the distributions. Appendix C.2 provides further details on the assumptions and their necessity.

Under these assumptions, we aim to identify the causal variables from high-dimensional observations. As shown by Lippe et al. (2022b), multidimensional causal variables are not always identifiable, since interventions can potentially only affect a subset of the variables dimensions. Thus, we are limited to identifying the intervention-dependent parts of variables, *i.e.* the *minimal causal variables*.

In particular, we learn an invertible mapping, $g_\theta : \mathcal{X} \rightarrow \mathcal{Z}$, from observations \mathcal{X} to a latent space $\mathcal{Z} \in \mathbb{R}^M$ with M dimensions. The latent space is structured by an assignment function $\psi : \llbracket 1..M \rrbracket \rightarrow \llbracket 0..K \rrbracket$ mapping each dimension of \mathcal{Z} to a causal factor C_1, \dots, C_K . We index the set of latent variables that ψ assigns to the causal factor C_i with $z_{\psi_i} = \{z_j | j \in \llbracket 1..M \rrbracket, \psi(j) = i\}$. Thereby, we use z_{ψ_0} to summarize all latents that model the noise E_o^t and the intervention-independent parts of all causal variables. Furthermore, to model the instantaneous causal relations, we learn a directed, acyclic graph G on the K latent variable groups $z_{\psi_0}, \dots, z_{\psi_K}$. The graph G induces a parent structure denoted by $z_{\psi_i}^{\text{pa}} = \{z_j | j \in \llbracket 1..M \rrbracket, \psi(j) \in \text{pa}_G(i)\}$ where we set $\text{pa}_G(0) = \emptyset$, *i.e.* the variables in z_{ψ_0} have no instantaneous parents. Meanwhile, the temporal causal graph, *i.e.* between C^t and C^{t+1} , is implicitly learned by conditioning the latent variables of a time step, z^{t+1} , on all latents of the previous time step, z^t . Since the orientations of the edges are known, *i.e.* from C^t to C^{t+1} , no causal discovery setup as for the instantaneous graph is strictly necessary, and the temporal graph can instead be pruned in a post-processing step. Overall, this results in the following prior over the latent variables:

$$p_{\phi, G}(z^{t+1} | z^t, I^{t+1}) = p_\phi(z_{\psi_0}^{t+1} | z^t) \cdot \prod_{i=1}^K p_\phi(z_{\psi_i}^{t+1} | z^t, z_{\psi_i}^{\text{pa}, t+1}, I_i^{t+1}) \quad (1)$$

Under interventions, we mask out the parents z^t and $z_{\psi_i}^{\text{pa}, t+1}$ for the prior of z^{t+1} , maintaining the independence relations under perfect interventions. Given a dataset of triplets $\{x^t, x^{t+1}, I^{t+1}\}$ with observations $x^t, x^{t+1} \in \mathcal{X}$ and intervention targets I^{t+1} , the full likelihood objective becomes:

$$p_{\phi, \theta, G}(x^{t+1} | x^t, I^{t+1}) = |\det J_{g_\theta}(x^{t+1})| p_{\phi, G}(z^{t+1} | z^t, I^{t+1}) \quad (2)$$

where the Jacobian of the invertible map g_θ , $|\det J_{g_\theta}(x^{t+1})|$, is introduced due to the change of variables of x to z . Under this setup, we derive the following identifiability result:

Theorem 3.2. *Suppose that ϕ^* , θ^* , ψ^* and G^* are the parameters that, under the constraint of maximizing the likelihood $p_{\phi, \theta, G}(x^{t+1} | x^t, I^{t+1})$, maximize the information content of $p_\phi(z_{\psi_0}^{t+1} | z^t)$ and minimize the edges in G^* . Then, with sufficient latent dimensions, the model ϕ^*, θ^*, ψ^* learns a latent structure where $z_{\psi_i}^{t+1}$ models the minimal causal variable of C_i , and G^* is the true instantaneous graph between these variables. Removing edges based on conditional independencies between time steps t and $t + 1$ identifies the true temporal graph. Finally, z_{ψ_0} models all remaining information.*

The proof for this theorem in Appendix C follows three main steps. First, we show that the true disentanglement function constitutes a global optimum of the likelihood objective of Equation (2), but is not necessarily unique. Second, we derive that any global optimum must have disentangled the minimal causal variables in the latent representation. Finally, we show that under this disentanglement, optimizing the likelihood of the observational and interventional data identifies the complete causal graph, *i.e.* instantaneous and temporal, between the minimal causal variables.

Intuitively, this theorem shows that we can indeed identify and disentangle the minimal causal variables, even when instantaneous effects are present. Furthermore, we are able to find the instantaneous causal graph G^* between the minimal causal variables, which, however, might not be exactly the same as the causal graph G_C between the true causal variables C_1^t, \dots, C_K^t . In particular, every edge $z_{\psi_i}^t \rightarrow z_{\psi_j}^t$ in G^* implies an edge $C_i^t \rightarrow C_j^t$ in G_C . However, some edges in G_C might be modeled by relations between intervention-independent parts of causal variables, which are captured by an edge $z_{\psi_0}^t \rightarrow z_{\psi_j}^t$ in G^* . Still, translating the edges from G^* to G_C following the previous implication does not introduce any wrong edge or orientation that was not present in G_C .

4 Causal representation learning with instantaneous effects

Based on the theoretical results presented above, we propose iCITRIS, a causal representation learning method that simultaneously identifies the causal variables and the instantaneous causal graph between them. Inspired by CITRIS (Lippe et al., 2022b), iCITRIS implements the mapping from observations to latent space either by a variational autoencoder (VAE) (Kingma and Welling, 2014) or by a normalizing flow (Rezende and Mohamed, 2015) trained on the representations of a pretrained autoencoder. In both cases, the disentanglement of the causal variables in latent space is promoted by enforcing the structure of Equation (1). However, crucially, the instantaneous graph G^* must be learned jointly with the causal representations, as we describe in the next subsections.

4.1 Learning the instantaneous causal graph

To learn the instantaneous causal graph simultaneously with the causal representation, we incorporate recent differentiable, score-based causal discovery methods in iCITRIS. Given a prior distribution over graphs $p(G)$, the prior distribution over the latent variables z^{t+1} of Equation (1) becomes:

$$p_\phi(z^{t+1}|z^t, I^{t+1}) = p_\phi(z_{\psi_0}^{t+1}|z^t) \cdot \mathbb{E}_G \left[\prod_{i=1}^K p_\phi(z_{\psi_i}^{t+1}|z^t, z_{\psi_i}^{t+1, \text{pa}}, I_i^{t+1}) \right] \quad (3)$$

where the parent sets, $z_{\psi_i}^{t+1, \text{pa}}$, depend on the graph structure G . The goal is to jointly optimize p_ϕ and $p(G)$ under maximizing the likelihood objective of Equation (2), such that $p(G)$ is peaked at the correct causal graph. To apply causal discovery methods in this setup, we consider each group of latents, $z_{\psi_i}^{t+1}$, as the potentially multidimensional causal factor C_i , on which the graphs must be recovered. To this end, we experiment with two different discovery methods: NOTEARS (Zheng et al., 2018), and ENCO (Lippe et al., 2022a).

NOTEARS (Zheng et al., 2018) casts structure learning as a continuous optimization problem by providing a continuous constraint to enforce acyclicity. Specifically, an adjacency matrix A is acyclic if the following holds: $c(A) = \text{tr}(\exp(A \circ A)) - K = 0$, where \circ is the Hadamard product, $\exp(\dots)$ the matrix exponential, and K the number of causal variables. To adapt NOTEARS to representation learning, we model the adjacency matrix with independent edge likelihoods, and differentially sample from it using the Gumbel-Softmax trick (Jang et al., 2017). We use these samples as graphs in the prior $p_\phi(z^{t+1}|z^t, I^{t+1})$ to mask the parents of the individual causal variables, and obtain gradients for the graph through the maximum likelihood objective of the prior. In order to promote acyclicity, we use the constraint $c(A)$ as a regularizer, and exponentially increase its weight over training. This ensures that at the end of the training, $c(A)$ is close to zero, and, thus, the predicted graph is acyclic.

ENCO (Lippe et al., 2022a), on the other hand, uses interventional data and a different graph parameterization to obtain acyclic graphs. The graph parameters are split into two sets: one for modeling the orientation per edge, and one for whether the edge exists or not. By using solely adjacent interventions to update the orientation parameters, Lippe et al. (2022a) show that ENCO naturally converges to the true, acyclic graph in the sample limit. Since iCITRIS requires interventions on variables that have potential edges of unknown orientations, we can integrate ENCO without additional constraints on the dataset. Instead of the Gumbel-Softmax trick, ENCO uses low-variance, unbiased gradients based on REINFORCE (Williams, 1992) to update the graph parameters, potentially providing a more stable optimization than NOTEARS. For efficiency, we merge the distribution and graph learning stage of ENCO, and update both the graph and distribution parameters at each iteration.

4.2 Stabilizing the optimization process

The main challenge in iCITRIS is that simultaneously identifying the causal variables and their graph leads to a chicken-and-egg situation: without knowing the variables, we cannot identify the graph; but without knowing the graph, we cannot disentangle the causal variables. This can cause the optimization to be naturally unstable and to converge to local minima with incorrect graphs. To stabilize the optimization process, we propose the following two approaches.

Graph learning scheduler During the first training iterations, the assignment of latent to causal variables is almost uniform, such that the gradients for the graph parameters are very noisy and uninformative. Thus, we use a learning rate schedule for the graph learning parameters such that the graph parameters are frozen for the first couple of epochs. During those training iterations, the model learns to fit the latent variables to the intervention variables under an arbitrary graph, leading to an initial, rough assignment of latent to causal variables. Then, we warm up the learning rate to slowly start the graph learning process while continuing to disentangle the causal variables in latent space.

Mutual information estimator Since iCITRIS requires perfect interventions to guarantee disentanglement of the causal variables, we can further exploit this information in the optimization process by enforcing independencies between parents and children under interventions. In particular, under interventions on the variable C_i at time t , *i.e.* $I_i^t = 1$, the following independencies must hold: $C_i^t \perp\!\!\!\perp \text{pa}(C_i^t) | I_i^t = 1$. The same independencies can be transferred to the latent space as $z_{\psi_i}^t \perp\!\!\!\perp (z_{\psi_i}^{t, \text{pa}}, z^{t-1}) | I_i^t = 1$. To use these independencies as learning signals in iCITRIS’s gradient-based framework, we use the fact that two variables being independent corresponds to the mutual

information (MI) of both to be zero (Kullback, 1997). Following previous work on neural network based MI estimation (Belghazi et al., 2018; Hjelm et al., 2019; van den Oord et al., 2018), we implement this framework by training a network to distinguish between samples from the joint distribution $p(z_{\psi_i}^t, z_{\psi_i^{\text{pa}}}^t, z^{t-1} | I_i^t = 1)$ and the product of their marginals, i.e. $p(z_{\psi_i}^t | I_i^t = 1)p(z_{\psi_i^{\text{pa}}}^t, z^{t-1} | I_i^t = 1)$. While the MI estimator network is trained to optimize its classification accuracy, the latents are optimized to do the opposite, effectively minimizing the mutual information between $z_{\psi_i}^t$ and its parents. This way, we regularize the latent representation to follow the independencies between causal variables and their parents under interventions.

5 Experiments

We evaluate iCITRIS on three videos datasets with varying difficulties and compare it to common disentanglement methods. We include further details for reproducibility in the appendix.

5.1 Experimental settings

Baselines Since iCITRIS is, to the best of our knowledge, the first method to identify causal variables with instantaneous effects in this setting, we compare it to methods for disentangling conditionally independent causal variables. Firstly, we use CITRIS (Lippe et al., 2022b) and the Identifiable VAE (iVAE) (Khemakhem et al., 2020a), which both assume that the variables are independent given the previous time step and intervention targets. Additionally, to also compare to a model with dependencies among latent variables, we evaluate the iVAE with an autoregressive prior, which we denote with iVAE-AR. To ensure comparability, we share the general model setup where possible (e.g. encoder/decoder network) across all methods. Appendix E discusses further hyperparameters.

Evaluation metrics To evaluate the identification of the causal factors, we follow Lippe et al. (2022b) and report the R^2 correlation scores between the true causal factors and the latent variables that have been assigned to a specific causal variable by the learned model. We denote the average correlation of the predicted causal factor to its true value with $R^2\text{-diag}$ (optimal 1), and the maximum correlation besides its true factor with $R^2\text{-sep}$ (optimal 0). Furthermore, to investigate the modeling of the temporal and instantaneous relations between the causal factors, we perform causal discovery as a post-processing step on the latent representations of all models, and report the structural hamming distance (SHD) between the predicted and true causal graph.

5.2 2D colored cells with causal effects: Voronoi benchmark

We first conduct experiments on synthetically generated causal graphs with various structures to investigate the difficulty and challenges of the task. We consider three instantaneous graph structures: *random* has a randomly sampled, acyclic graph structure with a likelihood of 0.5 of two variables being connected by a direct edge, and *chain* and *full* represent the minimally- and maximally-connected DAGs respectively. For each graph, we sample temporal edges at random with an edge likelihood of 0.25 between any pair of variables in C^t and C^{t+1} . Based on these graphs, we create the variable’s observational distributions as Gaussians parameterized by randomly initialized neural networks, and provide single-target, perfect interventions for all variables. The causal variables are mapped to image space \mathcal{X} by firstly applying a randomly initialized, two-layer normalizing flow to entangle the variables, and afterwards plotting them as colors in a 32x32 pixels image of a fixed Voronoi diagram as an irregular structure. Thus, the representation learning models need to distinguish between the entanglement by the random normalizing flow and the underlying causal graphs to identify the causal variables, while also performing causal discovery to find the correct causal graph.

In Figure 2, we show the results of all models on graphs of 4, 6, and 9 variables. For the *random* and *chain* graphs, iCITRIS-ENCO identifies the causal variables and their causal graph with only minor errors, even for the largest graphs of 9 variables. Even on the challenging *full* graph, iCITRIS-ENCO considerably outperforms the other models. In contrast, iCITRIS-NOTEARS struggles with the edge orientations and converges to edge likelihoods noticeably lower than 1.0, with which the variables can not be perfectly disentangled anymore, especially for increasing graph sizes. Meanwhile, CITRIS and iVAE find K conditionally independent dimensions in the data instead of the true causal variables, which leads to sparse instantaneous, but wrongly dense temporal graphs. Finally, the autoregressive baseline, iVAE-AR, naturally entangles all dimensions in the latent space, on which

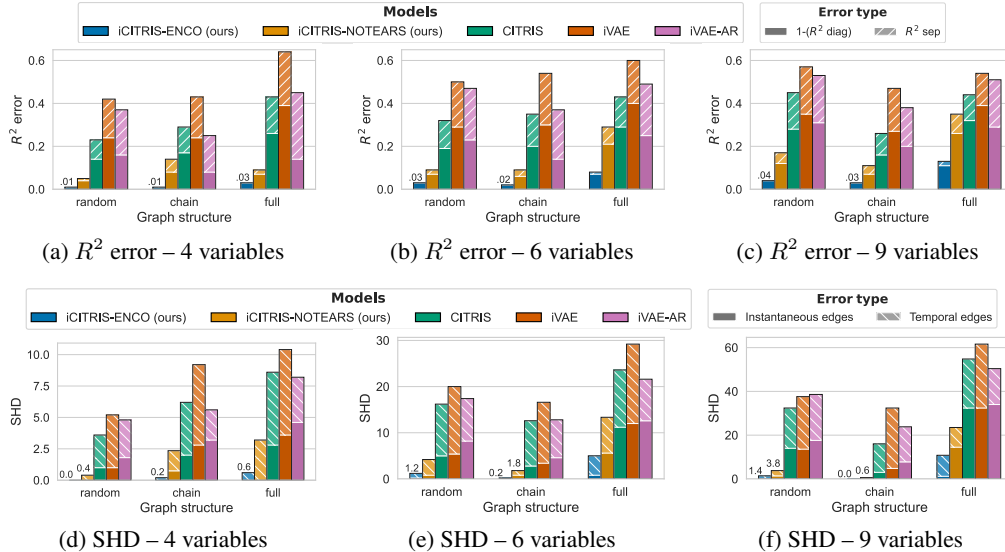


Figure 2: Results on the Voronoi benchmark over three graph structures and sizes with five seeds (error bars in Appendix F.1). For all metrics, lower is better. **Top row** (a-c): Plotting the R^2 correlation error as the average distance between predicted and true causal factors ($1-R^2$ diag", filled color), plus the maximum correlation to any other variable (" R^2 sep", striped). iCITRIS-ENCO performs well across graph structures and sizes. **Bottom row** (d-f): The SHD between predicted and ground truth causal graph, divided into instantaneous (filled bars) and temporal (striped bars) edges. iCITRIS-ENCO obtains the lowest error across graphs, with close to zero for the graphs random and chain.

Table 1: Results on Instantaneous Temporal Causal3DIdent over three seeds (standard deviations in Table 9). iCITRIS-ENCO performs best in identifying the variables and their graph.

Model	R^2 (diag \uparrow / sep \downarrow)	SHD (instant \downarrow / temp \downarrow)
iCITRIS-ENCO	0.96 / 0.05	1.33 / 5.00
iCITRIS-NOTEARS	0.95 / 0.09	4.00 / 5.00
CITRIS	0.92 / 0.19	4.67 / 10.00
iVAE	0.82 / 0.20	6.67 / 15.33
iVAE-AR	0.79 / 0.29	11.00 / 12.67

the true causal graph cannot be recovered anymore. This underlines the non-triviality of disentangling instantaneously-related causal variables. In conclusion, iCITRIS identifies the causal variables and their graph well across different graph structures and sizes, with ENCO outperforming NOTEARS due to more stable optimization, especially for larger, complex graphs.

5.3 3D object renderings: Instantaneous Temporal Causal3DIdent

As a visually challenging dataset, we use the Temporal Causal3DIdent dataset (von K \ddot{u} gelgen et al., 2021; Lippe et al., 2022b) which contains 3D renderings (64×64 pixels) of different object shapes under varying positions, rotations, and lights. To introduce instantaneous effects into the dataset, we replace all temporal relations with instantaneous edges, except those on the same variable ($C_i^t \rightarrow C_i^{t+1}$). For instance, a change in the rotation leads to an instantaneous change in the position of the object, which again influences the spotlight. Overall, we obtain an instantaneous graph of eight edges between the seven multidimensional causal variables. Since the dataset is visually complex, we use the normalizing flow variant of iCITRIS and CITRIS applied on a pretrained autoencoder.

Table 1 shows that iCITRIS-ENCO disentangles the causal variables well and recovers most instantaneous relations in this challenging setup, with one error on average. The temporal graph had more false positive edges due to minor, additional correlations. On the other hand, iCITRIS-NOTEARS struggles with the graph learning and incorrectly oriented edges during training, underlining the benefit of ENCO as the graph learning method in iCITRIS. The baselines have a significantly higher

Table 2: Results on the Causal Pinball dataset over three seeds (see Table 10 for standard deviations). Despite deterministic and sparse instantaneous effects, iCITRIS identifies the causal variables and graph of the Causal Pinball dataset well.

Model	R^2 (diag \uparrow / sep \downarrow)	SHD (instant \downarrow / temp \downarrow)
iCITRIS-ENCO	0.98 / 0.04	0.67 / 3.67
iCITRIS-NOTEARS	0.98 / 0.06	2.33 / 3.67
CITRIS	0.98 / 0.04	2.67 / 4.00
iVAE	0.55 / 0.04	2.33 / 4.33
iVAE-AR	0.53 / 0.15	4.33 / 6.33

entanglement of the causal variables and struggle with finding the true causal graph. In summary, iCITRIS-ENCO can identify the causal variables along with their instantaneous graph well, even in a visually challenging dataset.

5.4 Real game dynamics: Causal Pinball

Finally, we consider a simplified version of the game Pinball, which naturally comes with instantaneous causal effects: if the user activates the paddles when the ball is close, the ball is accelerated immediately. Similarly, when the ball hits a bumper, its light turns on and the score increases directly. This results in instantaneous effects under common frame rates. In this environment, we consider five causal variables: the position of the left paddle, the right paddle, the ball (position and velocity), the state of the bumpers, and the score. Pinball is closer to a real-world environment than the other two datasets and has two characteristic differences: (1) many aspects of the environment are deterministic, *e.g.* the ball movement, and (2) the instantaneous effects are sparse, *e.g.* the paddles do not influence the ball if it is far away of them. The first aspect violates assumptions of iCITRIS like faithfulness, questioning whether iCITRIS yet empirically works here.

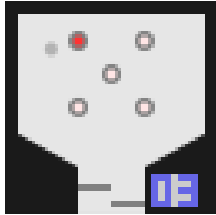


Figure 3: Example of Causal Pinball.

The results in Table 2 suggest that iCITRIS still works well on this environment. Besides disentangling the causal variables well, iCITRIS-ENCO identifies the instantaneous causal graph with minor errors. Interestingly, CITRIS obtains a good disentanglement score as well, which is due to the instantaneous effects being often sparse. Yet, there is still a gap between iCITRIS-ENCO and CITRIS in the instantaneous SHD, showing the benefit of learning the instantaneous graph jointly with the causal variables.

6 Conclusion

We propose iCITRIS, a causal representation learning framework for temporal intervened sequences with instantaneous effects. iCITRIS identifies the minimal causal variables while jointly learning the causal graph, including the instantaneous relations. In experiments, iCITRIS accurately recovers the causal factors and their graph in three different video datasets. While we envision a future application of methods similar to iCITRIS in a reinforcement learning setting, the limiting factor currently are the assumptions on the availability of perfect interventions with known targets. Future work includes investigating a setup where a sequence of actions is needed to perform targeted interventions (*e.g.* reaching a switch and flipping it). Finally, iCITRIS is limited to acyclic graphs, while for instantaneous causal effects cycles could occur under low frame rates, which is also an interesting future direction.

Acknowledgments and Disclosure of Funding

We thank Johann Brehmer and Pim de Haan for valuable discussions throughout the project. We also thank SURFsara for the support in using the Lisa Compute Cluster. This work is financially supported by Qualcomm Technologies Inc., the University of Amsterdam and the allowance Top consortia for Knowledge and Innovation (TKIs) from the Netherlands Ministry of Economic Affairs and Climate Policy.

References

- Mohamed Ishmael Belghazi, Aristide Baratin, Sai Rajeshwar, Sherjil Ozair, Yoshua Bengio, Aaron Courville, and Devon Hjelm. 2018. Mutual Information Neural Estimation. In *Proceedings of the 35th International Conference on Machine Learning*, volume 80 of *Proceedings of Machine Learning Research*, pages 531–540. PMLR.
- Blender Online Community. 2021. *Blender - a 3D modelling and rendering package*. Blender Foundation, Stichting Blender Foundation, Amsterdam.
- Johann Brehmer, Pim de Haan, Phillip Lippe, and Taco Cohen. 2022. Weakly supervised causal representation learning. *arXiv preprint arXiv:2203.16437*.
- Philippe Brouillard, Sébastien Lachapelle, Alexandre Lacoste, Simon Lacoste-Julien, and Alexandre Drouin. 2020. Differentiable Causal Discovery from Interventional Data. In *Advances in Neural Information Processing Systems 33: Annual Conference on Neural Information Processing Systems 2020, NeurIPS 2020, December 6-12, 2020, virtual*.
- Pierre Comon. 1994. Independent component analysis, A new concept? *Signal Processing*, 36(3):287–314.
- Thomas M. Cover and Joy A. Thomas. 2005. *Elements of Information Theory*. John Wiley and Sons, Ltd.
- Keenan Crane. 2021. Keenan’s 3D Model Repository. <https://www.cs.cmu.edu/~kmc Crane/Projects/ModelRepository/>.
- Brian Curless and Marc Levoy. 1996. **A Volumetric Method for Building Complex Models from Range Images**. In *Proceedings of the 23rd Annual Conference on Computer Graphics and Interactive Techniques, SIGGRAPH ’96*, page 303–312, New York, NY, USA. Association for Computing Machinery.
- Pim De Haan, Dinesh Jayaraman, and Sergey Levine. 2019. Causal confusion in imitation learning. *Advances in Neural Information Processing Systems*, 32.
- Thomas Dean and Keiji Kanazawa. 1989. **A model for reasoning about persistence and causation**. *Computational Intelligence*, 5(2):142–150.
- Vanessa Didelez, A. Philip Dawid, and Sara Geneletti. 2006. Direct and Indirect Effects of Sequential Treatments. In *Proceedings of the Twenty-Second Conference on Uncertainty in Artificial Intelligence, UAI’06*, page 138–146, Arlington, Virginia, USA. AUAI Press.
- Frederick Eberhardt. 2007. Causation and intervention. *Unpublished doctoral dissertation, Carnegie Mellon University*, page 93.
- Martin Engelcke, Adam R Kosiorek, Oivi Parker Jones, and Ingmar Posner. 2020. GENESIS: Generative scene inference and sampling with object-centric latent representations. *International Conference on Learning Representations (ICLR)*.
- William Falcon and The PyTorch Lightning team. 2019. **PyTorch Lightning**.
- Luigi Gresele, Julius von Kügelgen, Vincent Stimper, Bernhard Schölkopf, and Michel Besserve. 2021. Independent mechanism analysis, a new concept? In *Advances in Neural Information Processing Systems*.
- Kaiming He, Xiangyu Zhang, Shaoqing Ren, and Jian Sun. 2016. Deep residual learning for image recognition. In *Proceedings of the IEEE conference on computer vision and pattern recognition*, pages 770–778.
- R Devon Hjelm, Alex Fedorov, Samuel Lavoie-Marchildon, Karan Grewal, Phil Bachman, Adam Trischler, and Yoshua Bengio. 2019. Learning deep representations by mutual information estimation and maximization. In *International Conference on Learning Representations*.
- John D. Hunter. 2007. **Matplotlib: A 2D graphics environment**. *Computing in Science & Engineering*, 9(3):90–95.

- Antti Hyttinen, Frederick Eberhardt, and Patrik O Hoyer. 2013. Experiment selection for causal discovery. *Journal of Machine Learning Research*, 14:3041–3071.
- Aapo Hyvärinen, Juha Karhunen, and Erkki Oja. 2001. *Independent Component Analysis*. John Wiley & Sons.
- Aapo Hyvärinen and Hiroshi Morioka. 2016. Unsupervised Feature Extraction by Time-Contrastive Learning and Nonlinear ICA. In *Proceedings of the 30th International Conference on Neural Information Processing Systems, NIPS’16*, page 3772–3780, Red Hook, NY, USA. Curran Associates Inc.
- Aapo Hyvärinen, Hiroaki Sasaki, and Richard Turner. 2019. Nonlinear ICA Using Auxiliary Variables and Generalized Contrastive Learning. In *Proceedings of the Twenty-Second International Conference on Artificial Intelligence and Statistics*, volume 89 of *Proceedings of Machine Learning Research*, pages 859–868. PMLR.
- Sergey Ioffe and Christian Szegedy. 2015. Batch Normalization: Accelerating Deep Network Training by Reducing Internal Covariate Shift. In *Proceedings of the 32nd International Conference on Machine Learning*, volume 37 of *Proceedings of Machine Learning Research*, pages 448–456, Lille, France. PMLR.
- Eric Jang, Shixiang Gu, and Ben Poole. 2017. Categorical Reparameterization with Gumbel-Softmax. In *5th International Conference on Learning Representations, ICLR 2017, Toulon, France, April 24-26, 2017, Conference Track Proceedings*.
- Edward T. Jaynes. 1957. [Information Theory and Statistical Mechanics](#). *Phys. Rev.*, 106:620–630.
- Edwin T. Jaynes. 1968. [Prior Probabilities](#). *IEEE Transactions on Systems Science and Cybernetics*, 4(3):227–241.
- Ilyes Khemakhem, Diederik Kingma, Ricardo Monti, and Aapo Hyvarinen. 2020a. Variational Autoencoders and Nonlinear ICA: A Unifying Framework. In *Proceedings of the Twenty Third International Conference on Artificial Intelligence and Statistics*, volume 108 of *Proceedings of Machine Learning Research*, pages 2207–2217. PMLR.
- Ilyes Khemakhem, Ricardo Monti, Diederik Kingma, and Aapo Hyvarinen. 2020b. ICE-BeeM: Identifiable Conditional Energy-Based Deep Models Based on Nonlinear ICA. In *Advances in Neural Information Processing Systems*, volume 33, pages 12768–12778. Curran Associates, Inc.
- Diederik P. Kingma and Jimmy Ba. 2015. Adam: A Method for Stochastic Optimization. In *3rd International Conference on Learning Representations, ICLR 2015, San Diego, CA, USA, May 7-9, 2015, Conference Track Proceedings*.
- Diederik P. Kingma and Max Welling. 2014. Auto-Encoding Variational Bayes. In *2nd International Conference on Learning Representations, ICLR 2014, Banff, AB, Canada, April 14-16, 2014, Conference Track Proceedings*.
- Durk P Kingma and Prafulla Dhariwal. 2018. Glow: Generative Flow with Invertible 1x1 Convolutions. In *Advances in Neural Information Processing Systems*, volume 31. Curran Associates, Inc.
- Durk P Kingma, Tim Salimans, Rafal Jozefowicz, Xi Chen, Ilya Sutskever, and Max Welling. 2016. Improved variational inference with inverse autoregressive flow. *Advances in neural information processing systems*, 29.
- Thomas Kipf, Gamaleldin F Elsayed, Aravindh Mahendran, Austin Stone, Sara Sabour, Georg Heigold, Rico Jonschkowski, Alexey Dosovitskiy, and Klaus Greff. 2022. Conditional Object-Centric Learning from Video. *International Conference on Learning Representations (ICLR)*.
- David Klindt, Lukas Schott, Yash Sharma, Ivan Ustyuzhaninov, Wieland Brendel, Matthias Bethge, and Dylan Paiton. 2021. Towards Nonlinear Disentanglement in Natural Data with Temporal Sparse Coding. In *International Conference on Learning Representations (ICLR)*.
- Venkat Krishnamurthy and Marc Levoy. 1996. [Fitting Smooth Surfaces to Dense Polygon Meshes](#). In *Proceedings of the 23rd Annual Conference on Computer Graphics and Interactive Techniques, SIGGRAPH ’96*, page 313–324, New York, NY, USA. Association for Computing Machinery.

- Julius von Kügelgen, Yash Sharma, Luigi Gresele, Wieland Brendel, Bernhard Schölkopf, Michel Besserve, and Francesco Locatello. 2021. Self-Supervised Learning with Data Augmentations Provably Isolates Content from Style. In *Thirty-Fifth Conference on Neural Information Processing Systems*.
- Solomon Kullback. 1997. *Information theory and statistics*. Courier Corporation.
- Abhishek Kumar, Prasanna Sattigeri, and Avinash Balakrishnan. 2018. Variational Inference of Disentangled Latent Concepts from Unlabeled Observations. In *6th International Conference on Learning Representations, ICLR 2018, Vancouver, BC, Canada, April 30 - May 3, 2018, Conference Track Proceedings*.
- Sebastien Lachapelle, Pau Rodriguez, Rémi Le, Yash Sharma, Katie E Everett, Alexandre Lacoste, and Simon Lacoste-Julien. 2022. Disentanglement via Mechanism Sparsity Regularization: A New Principle for Nonlinear ICA. In *First Conference on Causal Learning and Reasoning*.
- Phillip Lippe, Taco Cohen, and Efstratios Gavves. 2022a. Efficient Neural Causal Discovery without Acyclicity Constraints. In *International Conference on Learning Representations*.
- Phillip Lippe, Sara Magliacane, Sindy Löwe, Yuki M. Asano, Taco Cohen, and Efstratios Gavves. 2022b. CITRIS: Causal Identifiability from Temporal Intervened Sequences. In *Proceedings of the 39th International Conference on Machine Learning, ICML 2022*.
- Francesco Locatello, Stefan Bauer, Mario Lucic, Gunnar Raetsch, Sylvain Gelly, Bernhard Schölkopf, and Olivier Bachem. 2019. Challenging Common Assumptions in the Unsupervised Learning of Disentangled Representations. In *Proceedings of the 36th International Conference on Machine Learning*, volume 97 of *Proceedings of Machine Learning Research*, pages 4114–4124. PMLR.
- Francesco Locatello, Ben Poole, Gunnar Rätsch, Bernhard Schölkopf, Olivier Bachem, and Michael Tschannen. 2020a. Weakly-Supervised Disentanglement Without Compromises. In *Proceedings of the 37th International Conference on Machine Learning, ICML 2020, 13-18 July 2020, Virtual Event*, volume 119 of *Proceedings of Machine Learning Research*, pages 6348–6359. PMLR.
- Francesco Locatello, Michael Tschannen, Stefan Bauer, Gunnar Rätsch, Bernhard Schölkopf, and Olivier Bachem. 2020b. Disentangling Factors of Variations Using Few Labels. In *International Conference on Learning Representations*.
- Francesco Locatello, Dirk Weissenborn, Thomas Unterthiner, Aravindh Mahendran, Georg Heigold, Jakob Uszkoreit, Alexey Dosovitskiy, and Thomas Kipf. 2020c. [Object-Centric Learning with Slot Attention](#). In *Advances in Neural Information Processing Systems*, volume 33, pages 11525–11538. Curran Associates, Inc.
- Ricardo Pio Monti, Kun Zhang, and Aapo Hyvärinen. 2019. Causal Discovery with General Non-Linear Relationships using Non-Linear ICA. In *Proceedings of the Thirty-Fifth Conference on Uncertainty in Artificial Intelligence, UAI 2019, Tel Aviv, Israel, July 22-25, 2019*, volume 115 of *Proceedings of Machine Learning Research*, pages 186–195. AUAI Press.
- Kevin Murphy. 2002. *Dynamic Bayesian Networks: Representation, Inference and Learning*. UC Berkeley, Computer Science Division.
- Martin Edward Newell. 1975. *The Utilization of Procedure Models in Digital Image Synthesis*. Ph.D. thesis, The University of Utah. AAI7529894.
- Aäron van den Oord, Yazhe Li, and Oriol Vinyals. 2018. [Representation Learning with Contrastive Predictive Coding](#). *CoRR*, abs/1807.03748.
- Adam Paszke, Sam Gross, Francisco Massa, Adam Lerer, James Bradbury, Gregory Chanan, Trevor Killeen, Zeming Lin, Natalia Gimelshein, Luca Antiga, Alban Desmaison, Andreas Köpf, Edward Yang, Zachary DeVito, Martin Raison, Alykhan Tejani, Sasank Chilamkurthy, Benoit Steiner, Lu Fang, Junjie Bai, and Soumith Chintala. 2019. PyTorch: An Imperative Style, High-Performance Deep Learning Library. In *Advances in Neural Information Processing Systems 32: Annual Conference on Neural Information Processing Systems 2019, NeurIPS 2019, December 8-14, 2019, Vancouver, BC, Canada*, pages 8024–8035.

- Judea Pearl. 2009. *Causality: Models, Reasoning and Inference*, 2nd edition. Cambridge University Press, USA.
- Emil Praun, Adam Finkelstein, and Hugues Hoppe. 2000. Lapped Textures. In *Proceedings of ACM SIGGRAPH 2000*, pages 465–470.
- Prajit Ramachandran, Barret Zoph, and Quoc V Le. 2017. Searching for activation functions. *arXiv preprint arXiv:1710.05941*.
- Daniilo Jimenez Rezende and Shakir Mohamed. 2015. Variational Inference with Normalizing Flows. In *Proceedings of the 32nd International Conference on Machine Learning, ICML 2015, Lille, France, 6-11 July 2015*, volume 37 of *JMLR Workshop and Conference Proceedings*, pages 1530–1538. JMLR.org.
- Szymon Rusinkiewicz, Doug DeCarlo, Adam Finkelstein, and Anothony Santella. 2021. Suggestive Contour Gallery. <https://gfx.cs.princeton.edu/proj/sugcon/models/>.
- Bernhard Schölkopf, Francesco Locatello, Stefan Bauer, Nan Rosemary Ke, Nal Kalchbrenner, Anirudh Goyal, and Yoshua Bengio. 2021. Toward causal representation learning. *Proceedings of the IEEE*, 109(5):612–634.
- Maximilian Seitzer, Bernhard Schölkopf, and Georg Martius. 2021. Causal influence detection for improving efficiency in reinforcement learning. *Advances in Neural Information Processing Systems*, 34.
- Peter Sorrenson, Carsten Rother, and Ullrich Köthe. 2020. Disentanglement by Nonlinear ICA with General Incompressible-flow Networks (GIN). In *International Conference on Learning Representations*.
- P. Spirtes, C. Glymour, and R. Scheines. 2000. *Causation, Prediction, and Search*, 2nd edition. MIT Press, Cambridge MA.
- Frederik Träuble, Elliot Creager, Niki Kilbertus, Francesco Locatello, Andrea Dittadi, Anirudh Goyal, Bernhard Schölkopf, and Stefan Bauer. 2021. On Disentangled Representations Learned from Correlated Data. In *Proceedings of the 38th International Conference on Machine Learning*, volume 139 of *Proceedings of Machine Learning Research*, pages 10401–10412. PMLR.
- Greg Turk and Marc Levoy. 1994. [Zippered Polygon Meshes from Range Images](#). In *Proceedings of the 21st Annual Conference on Computer Graphics and Interactive Techniques, SIGGRAPH '94*, page 311–318, New York, NY, USA. Association for Computing Machinery.
- Ronald J. Williams. 1992. Simple statistical gradient-following algorithms for connectionist reinforcement learning. In *Machine Learning*, pages 229–256.
- Mengyue Yang, Furui Liu, Zhitang Chen, Xinwei Shen, Jianye Hao, and Jun Wang. 2021. CausalVAE: disentangled representation learning via neural structural causal models. In *Proceedings of the IEEE/CVF Conference on Computer Vision and Pattern Recognition*, pages 9593–9602.
- Weiran Yao, Yuewen Sun, Alex Ho, Changyin Sun, and Kun Zhang. 2022. Learning Temporally Causal Latent Processes from General Temporal Data. In *International Conference on Learning Representations*.
- Junzhe Zhang, Daniel Kumor, and Elias Bareinboim. 2020. Causal imitation learning with unobserved confounders. *Advances in neural information processing systems*, 33:12263–12274.
- Xun Zheng, Bryon Aragam, Pradeep Ravikumar, and Eric P. Xing. 2018. DAGs with NO TEARS: Continuous Optimization for Structure Learning. In *Advances in Neural Information Processing Systems 31: Annual Conference on Neural Information Processing Systems 2018, NeurIPS 2018, December 3-8, 2018, Montréal, Canada*, pages 9492–9503.
- Roland S. Zimmermann, Yash Sharma, Steffen Schneider, Matthias Bethge, and Wieland Brendel. 2021. Contrastive Learning Inverts the Data Generating Process. In *Proceedings of the 38th International Conference on Machine Learning, ICML 2021, 18-24 July 2021, Virtual Event*, volume 139 of *Proceedings of Machine Learning Research*, pages 12979–12990. PMLR.

Supplementary material
iCITRIS: Causal Representation Learning for
Instantaneous Temporal Effects

TABLE OF CONTENTS

A Broader Impact	15
B Reproducibility statement	15
C Proofs	16
C.1 Preliminaries	16
C.2 Assumptions for Identifiability	18
C.3 Theorem 3.2 - Proof outline	22
C.4 Theorem 3.2 - Proof Step 1: The true model is a global optimum of the likelihood objective	23
C.5 Theorem 3.2 - Proof Step 2: Characterizing the disentanglement class	25
C.6 Theorem 3.2 - Proof Step 3: Identifiability of the causal graph	29
C.7 Theorem 3.2 - Proof Step 4: Final identifiability result	31
D Datasets	33
D.1 Voronoi benchmark	33
D.2 Instantaneous Temporal Causal3DIdent	35
D.3 Causal Pinball	36
E Experimental details	38
E.1 iCITRIS - Model details	38
E.2 Hyperparameters	40
E.3 Evaluation metrics	41
F Additional experimental results	43
F.1 Voronoi benchmark	43
F.2 Instantaneous Temporal Causal3DIdent experiments	46
F.3 Causal Pinball	46

A Broader Impact

The importance of causal reasoning for machine learning applications, especially reinforcement learning and latent dynamics understanding, has been emphasized by several previous works (De Haan et al., 2019; Lachapelle et al., 2022; Pearl, 2009; Schölkopf et al., 2021; Seitzer et al., 2021; Zhang et al., 2020). Thereby, starting from low-level information like pixels constitutes a considerable challenge, since we aim at reasoning about objects and abstract concepts instead of low-level pixels. We believe that this work contributes an important step towards tackling this challenge since it goes beyond previous work by considering instantaneous effects, a common property in real-world systems. Besides providing theoretical identifiability results, we also propose a practical algorithm with which one can learn the causal variables and their graph from high-level observations. Furthermore, we envision a reinforcement learning setting as a future application, where a robotic system may be able to interact with an environment. However, the main assumption that prevent us from doing this so far, is the availability of perfect interventions for which the intervention targets are known. In many systems, one might not be able to directly perform such interventions, but rather require several steps of low-level actions. For instance, instead of being provided the intervention targets, future work could consider a robotic setup where one can control a robot arm which can perform several interactions (*e.g.*, flipping a switch), and we believe that our work can constitute the starting point for such extension. Moreover, as we have seen in the experiments on the Causal Pinball environment, not all assumptions must be strictly fulfilled to identify the variables empirically, showing that iCITRIS is more widely applicable than just in the ideal theoretical setting. Moving towards this empirical goal, recent advances in unsupervised object-centric learning (Engelcke et al., 2020; Kipf et al., 2022; Locatello et al., 2020c) have shown that objects, which can often be considered as groups of causal variables like position and velocity, can be identified from high-dimensional data without labels. A possible combination of such object-centric approaches with our causal representation learning method can relax further assumptions by using the objects as a prior disentanglement of information, opening up further possible applications of iCITRIS. Thus, we believe that this work contributes an important step towards practical causal representation learning methods, and can form the basis of several future works.

Since the possible applications of causal representation learning and specifically iCITRIS are fairly wide-ranging, there might be potential impacts we cannot forecast at the current time. This includes misuses of the method for unethical purposes. For instance, an incorrect application of the method can be used to justify false causal relations, such as referencing gender and race as causes for other characteristics of a person. Hence, the obligation to use this method in a correct way within ethical boundaries lies on the user, and the outputs of the method should always be critically evaluated. We will emphasize this responsibility of the user in the public license of our code.

B Reproducibility statement

For reproducibility, the code for all models used in this paper is publicly available at <https://github.com/phlippe/CITRIS>. Further, we provide the code for generating the Voronoi benchmark, the Instantaneous Temporal Causal3DIdent dataset, and the Causal Pinball environment. More details on the datasets and visualizations are outlined in Appendix D.

Moreover, for all experiments of Section 5, we have included a detailed overview of the hyperparameters in E.2 and additional implementation details of the evaluation metrics and model architecture components in Appendix E.1. All experiments have been repeated for at least 3 seeds (5 seeds for the Voronoi benchmark) to obtain stable, reproducible results. We provide an overview of the standard deviations, as well as additional results in Appendix F.

Finally, all experiments in this paper were performed on a single NVIDIA TitanRTX GPU with a 6-core CPU. The overall computation time of all experiments together in this paper correspond to approximately 80 GPU days (excluding hyperparameter search and trials during the research).

C Proofs

In this section, we provide the proof for the identifiability theorem 3.2 in Section 3 and Lemma 3.1. The section is structured into three main parts. First, in Appendix C.1, we give an overview of the notation and elements that are used in the proof. Next, we discuss the assumptions needed for Theorem 3.2, with a focus on why they are needed and what a violation of these assumptions can cause. Additionally, we provide a proof of Lemma 3.1 in this subsection. Finally, we provide the proof of Theorem 3.2, structured into multiple subsections as different main steps of the proof. A detailed overview of the proof is provided in Appendix C.3.

C.1 Preliminaries

To clarify the used notation and definitions in the proof, we first discuss the definitions of the properties of causal models. Next, we review the used notation for all other elements in the proof.

C.1.1 Causal model definition

Given a causal graph $\mathcal{G} = (V, E)$, each node $i \in V$ is associated with a causal variable C_i , which can be scalar or vector valued. Each edge $(i, j) \in E$ represents a causal relation from C_i to C_j : $C_i \rightarrow C_j$, where C_i is a *parent* of C_j and $\text{pa}_{\mathcal{G}}(C_i)$ are all parents of C_i in \mathcal{G} . We can cluster multiple causal variables C_1, \dots, C_K in a single variable $C = (C_1, \dots, C_K)$. C then inherits all incoming and outgoing edges from its components C_i for $i = 1, \dots, K$. We assume that the underlying latent causal process is a dynamic Bayesian network (DBN) (Dean and Kanazawa, 1989; Murphy, 2002) G over (C_1, C_2, \dots, C_K) that is first-order Markov, stationary, and without instantaneous effects. This means that in G each causal factor C_i is instantiated at each time step t , denoted by C_i^t , and its causal parents can only be causal factors at time $t - 1$, denoted as C_j^{t-1} , including its own previous value C_i^{t-1} , and factors at time t , excluding its own value. In other words, for $t = 1, \dots, T$ and for each causal factor $i = 1, \dots, K$ we can model $C_i^t = f_i(\text{pa}_{\mathcal{G}}(C_i^t), \epsilon_i)$, where $\text{pa}_{\mathcal{G}}(C_i^t) \subseteq \{C_1^{t-1}, \dots, C_K^{t-1}, C_1^t, \dots, C_{i-1}^t, C_{i+1}^t, \dots, C_K^t\}$. We also assume all ϵ_i for $i = 1, \dots, K$ are mutually independent noises. To represent a DBN, the graph structure must be acyclic. This means that there does not exist a directed path in \mathcal{G} from any node C_i^t back to itself. Further, the structure of the graph is time-invariant, *i.e.*, $\text{pa}_{\mathcal{G}}(C_i^t) = \text{pa}_{\mathcal{G}}(C_i^1)$ for any $t = 1, \dots, T$.

We use a binary intervention vector $I^t \in \{0, 1\}^K$ to indicate that a variable C_i^t in G is intervened upon if and only if $I_i^t = 1$. We consider that the intervention vector components I_i^t might be confounded by another $I_j^t, i \neq j$, and represent these dependencies with an unobserved regime variable R^t , which is similar to “policy variables” in Spirtes et al. (2000) or “regime indicators” in Didelez et al. (2006). We augment the underlying causal graph \mathcal{G} with the intervention variable I_i^t associated with each causal factor C_i^t by including it in its parent set: $\text{pa}_{G'}(C_i^t) = \text{pa}_{\mathcal{G}}(C_i^t) \cup \{I_i^t\}$. Each intervened variable C_j^t in a time step will have its corresponding intervention variable I_j^t set to 1, otherwise the intervention variable will be set to 0 if the causal factor is not intervened upon at the time step t . We say that a distribution p is *Markov* w.r.t. the augmented DAG G' if it factors as $p(V^t) = \prod_{j \in V'} p(V_j | \text{pa}_{G'}(V_j))$, where V_j includes the causal factors C_i^t , the intervention vector components I_i^t , and the regime R^t . Moreover, we say that p is *faithful* to a causal graph G' , if there are no additional conditional independencies to the d-separations one can read from the graph G' . The augmented graph G' can model interventions with an arbitrary number of targets, including observational data. In this paper, we consider *soft* interventions (Eberhardt, 2007), in which the conditional distribution changes while potentially maintaining parent relations, *i.e.*, $p(C_i^t | \text{pa}_{\mathcal{G}}(C_i^t), I_i^t = 1) \neq p(C_i^t | \text{pa}_{\mathcal{G}}(C_i^t), I_i^t = 0)$, and *perfect* interventions (Pearl, 2009), which change a causal variable independent of its original parents, *i.e.*, $p(C_i^t | \text{pa}_{\mathcal{G}}(C_i^t), I_i^t = 1) = p(C_i^t | I_i^t = 1)$. The latter corresponds to a do-operation $\text{do}(C_i^t = c_i)$ in Pearl (2009), where c_i is randomly sampled from $p(C_i^t | I_i^t = 1)$.

C.1.2 Notation

Throughout the proof, we will use the same notation as used in the main paper, and try to align it as much as possible with Lippe et al. (2022b). As a summary, the notation is as follows:

- We denote the K causal factors in the latent causal dynamical system as C_1, \dots, C_K ;
- The dimensions and space of a causal variable is denoted as $C_i \in \mathcal{D}_i^{M_i}$ with $M_i \geq 1$ and let

- \mathcal{D}_i be \mathbb{R} for continuous variables (e.g., spatial position), \mathbb{Z} for discrete variables (e.g., the score of a player) or mixed;
- We group all causal factors in a single variable $C = (C_1, \dots, C_K) \in \mathcal{C}$, where \mathcal{C} is the causal factor space $\mathcal{C} = \mathcal{D}_1^{M_1} \times \mathcal{D}_2^{M_2} \times \dots \times \mathcal{D}_K^{M_K}$;
 - The data we base our identifiability on is generated by a latent Dynamic Bayesian network with variables $(C_1^t, C_2^t, \dots, C_K^t)_{t=1}^T$;
 - We assume to know at each time step the binary intervention vector $I^t \in \{0, 1\}^{K+1}$ where $I_i^t = 1$ refers to an intervention on the causal factor C_i^t . As a special case $I_0^t = 0$ for all t ;
 - For each causal factor C_i , there exists a split $s_i^{\text{var}}(C_i), s_i^{\text{inv}}(C_i)$ such that $s_i^{\text{var}}(C_i)$ represents the variable/manipulable part of C_i , while $s_i^{\text{inv}}(C_i)$ represents the invariable part of C_i ;
 - The minimal causal split is defined as the one which only contains the intervention-dependent information in $s_i^{\text{var}}(C_i)$, and everything else in $s_i^{\text{inv}}(C_i)$. This split is denoted by $s_i^{\text{var}^*}(C_i)$ and $s_i^{\text{inv}^*}(C_i)$;
 - At each time step, we can access observations $x^t, x^{t+1} \in \mathcal{X} \subseteq \mathbb{R}^N$;
 - There exist a bijective mapping between observations and causal/noise space, denoted by $h : \mathcal{C} \times \mathcal{E} \rightarrow \mathcal{X}$, where \mathcal{E} is the space of the noise variables;
 - The noise $E^t \in \mathcal{E}$ at a time step t subsumes all randomness besides the causal model which influences the observations. For example, this could be brightness shifts in Causal3D, or color shifts in the Causal Pinball environment since no causal factor is encoded in brightness and color in these setups respectively. While this setting is quite general, we still require that the values of the causal factors must be identifiable from single observations. Hence, the joint dimensionality of the noise and causal model is limited to the image size.
 - For any model learning a latent space, we denote the vector of latent variables by $z^t \in \mathcal{Z} \subseteq \mathbb{R}^M$, where \mathcal{Z} is the latent space of dimension $M \geq \dim(\mathcal{E}) + \dim(\mathcal{C})$;
 - In iCITRIS, we learn the inverse of the observation function as $g_\theta : \mathcal{X} \rightarrow \mathcal{Z}$;
 - In iCITRIS, we learn an assignment from latent dimensions to causal factors, denoted by $\psi : \llbracket 1..M \rrbracket \rightarrow \llbracket 0..K \rrbracket$;
 - The latent variables assigned to each causal factor C_i by ψ are denoted as $z_{\psi_i} = \{z_j | j \in \llbracket 1..M \rrbracket, \psi(j) = i\} = \{g_\theta(x^t)_j | j \in \llbracket 1..M \rrbracket, \psi(j) = i\}$;
 - The remaining latent variables that are not assigned to any causal factor are denoted as z_{ψ_0} ;
 - In iCITRIS, we learn a directed, acyclic graph $G = (V, E)$ where $V = \{z_{\psi_i} | i \in \llbracket 0..K \rrbracket\}$ and the edges represent directed causal relations;
 - The graph G induces a parent structure which we denote by $z_{\psi_i^{\text{pa}}} = \{z_j | j \in \llbracket 1..M \rrbracket, \psi(j) \in \text{pa}_G(i)\}$ where $\text{pa}_G(0) = \emptyset$, i.e. the variables in z_{ψ_0} having no instantaneous parents;
 - The parents of a causal variable within the same time step $t+1$ are denoted by $\text{pa}^{t+1}(C_i^{t+1})$, and the parents of the previous time step t by $\text{pa}^t(C_i^{t+1})$;
 - As a special case, we denote the function g_θ with the parameters θ that precisely model the inverse of the true observation function, h^{-1} , as the disentanglement function $\delta^* : \mathcal{X} \rightarrow \tilde{\mathcal{C}} \times \tilde{\mathcal{E}}$ with $\tilde{\mathcal{C}} = \mathcal{D}_1^{\tilde{M}_1} \times \dots \times \mathcal{D}_K^{\tilde{M}_K}$ and \tilde{M}_i being the number of latent dimensions assigned to the causal factor C_i by ψ^* . We denote the output of δ^* for an observation X as $\delta^*(X) = (\tilde{C}_1, \tilde{C}_2, \dots, \tilde{E})$. The representation of δ^* as a learnable function is denoted by g_θ^* and ψ^* ;
 - In the following proof, we will use entropy as a measure of information content in a random variable. To be invariant to possible invertible transformations, e.g. scaling by 2, we use the notion of the limiting density of discrete points (LDDP) (Jaynes, 1957, 1968). In contrast to differential entropy, LDDP introduces an *invariant measure* $m(X)$, which can be seen as a reference distribution we measure the entropy of $p(X)$ to. The entropy is thereby defined as:

$$H(X) = - \int p(X) \log \frac{p(X)}{m(X)} dx \quad (4)$$

In the following proof, we will consider entropy measures over latent and causal variables. For the latent variables, we consider $m(X)$ to be the push-forward distribution of an arbitrary, but fixed distribution in \mathcal{X} (e.g. random Gaussian if $\mathcal{X} = \mathbb{R}^n$) through g_θ . For the causal variables, we consider it to be the push-forward through h^{-1} . For more details on LDDP, see Lippe et al. (2022b, Appendix A.1.2) and Jaynes (1957, 1968).

C.2 Assumptions for Identifiability

In this section, we provide a detailed discussion of the assumptions of iCITRIS to enable the identification of an underlying causal graph with instantaneous effects. We thereby focus on why these assumptions are necessary, and how a violation of those can lead to scenarios where the causal variables and graph is not identifiable.

C.2.1 Assumption 1: The interventions on the causal variables are perfect

iCITRIS requires perfect interventions on the causal variables, in order to disentangle the variables in latent space. The perfect interventions are necessary to obtain samples in which the dependencies among the causal variables are broken, as stated in Lemma 3.1 and copied here for completeness:

Lemma C.1. *A causal variable C_i cannot always be uniquely identified in iTRIS if C_i has instantaneous parents and no perfect interventions on C_i have been observed.*

Proof. To prove this Lemma, it is sufficient to present a counterexample for which a variable C_i cannot be uniquely identified. Consider two random, causal variables C_1, C_2 with the causal graph $C_1^t \rightarrow C_1^{t+1}, C_2^t \rightarrow C_2^{t+1}$. The two causal variables C_1, C_2 have therefore no instantaneous relations. Further, consider the (soft-interventional) distributions $p_1(C_1^{t+1}|C_1^t, I_1^{t+1})$ and $p_2(C_2^{t+1}|C_2^t, I_2^{t+1})$ whose form can be arbitrary, but for this example, we choose them to be Gaussian with constant variance:

$$p_1(C_1^{t+1}|C_1^t, I_1^{t+1}) = \begin{cases} \mathcal{N}(C_1^{t+1}|\mu_1(C_1^t), \sigma_1(C_1^t)^2) & \text{if } I_1^{t+1} = 0 \\ \mathcal{N}(C_1^{t+1}|\tilde{\mu}_1(C_2^t), \tilde{\sigma}_1(C_1^t)^2) & \text{if } I_1^{t+1} = 1 \end{cases} \quad (5)$$

$$p_2(C_2^{t+1}|C_2^t, I_2^{t+1}) = \begin{cases} \mathcal{N}(C_2^{t+1}|\mu_2(C_2^t), \sigma_2(C_2^t)^2) & \text{if } I_2^{t+1} = 0 \\ \mathcal{N}(C_2^{t+1}|\tilde{\mu}_2(C_2^t), \tilde{\sigma}_2(C_2^t)^2) & \text{if } I_2^{t+1} = 1 \end{cases} \quad (6)$$

where $\mu_1, \tilde{\mu}_1, \mu_2, \tilde{\mu}_2, \sigma_1, \tilde{\sigma}_1, \sigma_2, \tilde{\sigma}_2$ are arbitrary, potentially non-linear functions of C_1^t and C_2^t respectively. Further, to consider the simplest case, suppose that the observation X^t at a time step t are the causal variables themselves, $X^t = [C_1^t, C_2^t]$, and we observe data points of all intervention settings, i.e. $I_i^{t+1} \sim \text{Bernoulli}(q)$ with $0 < q < 1$.

Under this setup, the true generative model follows the distribution:

$$p(X^{t+1}|X^t, I^{t+1}) = p(C_1^{t+1}, C_2^{t+1}|C_1^t, C_2^t, I_1^{t+1}, I_2^{t+1}) \quad (7)$$

$$= p(C_1^{t+1}|C_1^t, C_2^t, I_1^{t+1}, I_2^{t+1}) \cdot p(C_2^{t+1}|C_1^t, C_2^t, I_1^{t+1}, I_2^{t+1}) \quad (8)$$

$$= p_1(C_1^{t+1}|C_1^t, I_1^{t+1}) \cdot p_2(C_2^{t+1}|C_2^t, I_2^{t+1}) \quad (9)$$

where $C_1^{t+1} \perp\!\!\!\perp C_2^{t+1}|X^t, I^{t+1}$. To show that the causal variables are not uniquely identifiable, we need at least one other representation which can achieve the same likelihood as the true generative model under all intervention settings I^{t+1} . For this, consider the following distribution:

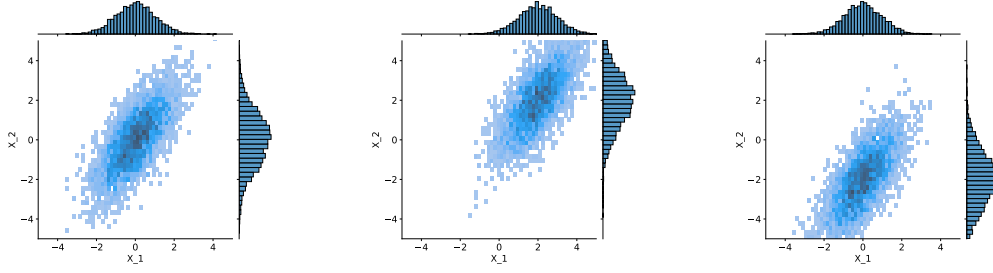
$$p(X^{t+1}|X^t, I^{t+1}) = p(C_1^{t+1}, C_2^{t+1}|C_1^t, C_2^t, I_1^{t+1}, I_2^{t+1}) \quad (10)$$

$$= p(C_1^{t+1}|C_1^t, C_2^t, I_1^{t+1}, I_2^{t+1}) \cdot p(C_2^{t+1}|C_1^t, C_2^t, C_1^{t+1}, I_1^{t+1}, I_2^{t+1}) \quad (11)$$

$$= p_1(C_1^{t+1}|C_1^t, I_1^{t+1}) \cdot \hat{p}_2(C_1^{t+1} + C_2^{t+1}|C_2^t, C_1^{t+1}, I_2^{t+1}) \quad (12)$$

$$= p_1(\hat{C}_1^{t+1}|C_1^t, I_1^{t+1}) \cdot \hat{p}_2(\hat{C}_2^{t+1}|C_2^t, \hat{C}_1^{t+1}, I_2^{t+1}) \quad (13)$$

with $\hat{C}_1^{t+1} = C_1^{t+1}, \hat{C}_2^{t+1} = C_1^{t+1} + C_2^{t+1}$. Note the additional dependency of \hat{C}_2^{t+1} on \hat{C}_1^{t+1} , which is possible in the space of possible causal models with an additional instantaneous causal edge



(a) Observational distribution $p(X^t|X^{t-1} = C, I_1^t = 0, I_2^t = 0)$ (b) Interventional distribution $p(X^t|X^{t-1} = C, I_1^t = 1, I_2^t = 0)$ (c) Interventional distribution $p(X^t|X^{t-1} = C, I_1^t = 0, I_2^t = 1)$

Figure 4: Example distribution for showcasing the necessity of perfect interventions for disentangling causal variables with instantaneous effects. Suppose we are given two-dimensional observations X^t , for which the observational and interventional distributions are plotted in (a)-(c). The central plot of each subfigure shows a 2D histogram, and the subplots above and on the right show the 1D marginal histograms. For simplicity, we keep the previous time step, X^{t-1} , constant here. From the interventional distribution, one might suggest that we have the latent causal graph $C_1 \rightarrow C_2$ since under $I_1^t = 1$, the distribution of both observational distributions change, while $I_2^t = 1$ keeps X_2 unchanged. However, the data has been actually generated from two independent causal variables, which have been entangled by having $X^t = [C_1^t, C_1^t + C_2^t]$. We cannot distinguish between these two latent models from interventions that do not reliably break instantaneous causal effects, showing the need for perfect interventions.

$\hat{C}_1^{t+1} \rightarrow \hat{C}_2^{t+1}$. The new distribution \hat{p}_2 is identical to the true distribution, since:

$$\hat{p}_2(C_1^{t+1} + C_2^{t+1}|C_2^t, C_1^{t+1}, I_2^{t+1} = 0) = \mathcal{N}(C_1^{t+1} + C_2^{t+1}|C_1^{t+1} + \mu_2(C_2^t), \sigma_2(C_2^t)^2) \quad (14)$$

$$= \frac{1}{\sqrt{2\pi}\sigma_2(C_2^t)} \exp\left(-\frac{1}{2} \frac{(C_1^{t+1} + C_2^{t+1} - (C_1^{t+1} + \mu_2(C_2^t)))^2}{\sigma_2(C_2^t)^2}\right) \quad (15)$$

$$= \frac{1}{\sqrt{2\pi}\sigma_2(C_2^t)} \exp\left(-\frac{1}{2} \frac{(C_2^{t+1} - \mu_2(C_2^t))^2}{\sigma_2(C_2^t)^2}\right) \quad (16)$$

$$= \mathcal{N}(C_2^{t+1}|\mu_2(C_2^t), \sigma_2(C_2^t)^2) \quad (17)$$

$$= p_2(C_2^{t+1}|C_2^t, I_2^{t+1} = 0) \quad (18)$$

Similarly, one can show that $\hat{p}_2(C_1^{t+1} + C_2^{t+1}|C_2^t, C_1^{t+1}, I_2^{t+1} = 1) = p_2(C_2^{t+1}|C_2^t, I_2^{t+1} = 1)$. Hence, the alternative representation $\hat{C}_1^{t+1}, \hat{C}_2^{t+1}$ can model the distribution $p(X^{t+1}|X^t, I^{t+1})$ as well as the true causal model. In conclusion, from the samples alone, we cannot distinguish between the two representation C_1, C_2 and \hat{C}_1, \hat{C}_2 , and the model is therefore not identifiable. \square

An alternative example with a non-trivial observation function is visualized in Figure 4, which further underlines the problem.

This shows that with soft interventions, one cannot distinguish between causal relations introduced by the observation function and those that are in the true causal model. Perfect interventions, however, provide an opportunity to do so since if we had known that the intervention on C_2 is perfect, the second causal model could not have modeled the correct distribution under $I_2 = 1$. This is since under interventions on a variable, all causal relations to its parents are broken, but only the relations introduced by the encoding function remain. Thus, we can distinguish between the two, allowing us to identify the correct causal model.

While we have shown that soft interventions are not sufficient for finding the instantaneous causal graph, this does not necessarily hold for the temporal relations. For instance, one might have interventions that are perfect within a time step, but keeps the dependency to the previous time step. However, for simplicity, we focus here on fully perfect interventions, and leave this relaxation to future work.

C.2.2 Assumption 2: Additional variables without interventions are not children of intervened variables

In practice, it may not be feasible to obtain interventions for every causal variable in a complex, dynamical system. Thus, we need to deal with having interventions on only a subgroup of the causal variables.

For those variables, we need to take the assumption that they are not children of the variables, for which we have observed interventions. The necessity of this assumption becomes clear when considering Appendix C.2.1, in which we have shown that soft interventions are not sufficient to tell apart entanglement introduced by the observation function, and entanglement induced by the causal relations. Coming back to the example of the proof in Appendix C.2.1, suppose that we have only given perfect interventions on C_1 , and not C_2 . From interventions on C_1 alone, we cannot distinguish between the true causal model and $\hat{C}_1^{t+1} = C_1^{t+1}$, $\hat{C}_2^{t+1} = C_1^{t+1} + C_2^{t+1}$ ($\hat{C}_1^{t+1} \rightarrow \hat{C}_2^{t+1}$ as causal graph), since the intervention on C_1 does not affect the entanglement and causal mechanism of \hat{C}_2^{t+1} . Thus, it is not possible to identify the causal variables and the respective graph if there may exist instantaneous effects from variables with interventions to those without. However, under the assumption that the variables without interventions have no instantaneous relation with the intervened variables, one can distinguish between the solely passively observed variables and those with perfect interventions, since all entanglement between those within a time step must come from the observation function, not the causal model. Still, among all causal variables without interventions, a disentanglement cannot be guaranteed without further assumptions due to the lack of observed change in their causal mechanism, and a causal graph among those may exist as well.

C.2.3 Assumption 3: The intervention targets are unique for each causal variable

iCITRIS builds upon interventions to identify the causal variables. The intervention targets are not necessarily independent of each other, but can be confounded. For instance, we could have a setting where we only obtain single-target interventions, or a certain variable C_i can only be jointly intervened upon with another variable C_j . In this large space of possible experimental settings, we naturally cannot guarantee identifiability all the time. In particular, we require that intervention targets for the different causal variables are unique:

Lemma C.2. *All information that is strictly dependent on the intervention target I_i^t , i.e. $s^{\text{var}}(C_i)$ - the minimal causal variable of C_i , cannot be disentangled from another causal variable, C_j with $j \neq i$, if their intervention targets are identical: $\forall t, I_i^t = I_j^t$.*

Proof. Lippe et al. (2022b) have shown that two causal variables C_i, C_j cannot be disentangled from observational data alone if they follow a Gaussian distribution with equal variance over time. Taking this setup, consider that additionally to observational data, we observe samples where both variables have been intervened upon, $I_i^{t+1} = I_j^{t+1} = 1$. If the interventional distribution of C_i and C_j are both Gaussian with the same variance, we have the same non-identifiability as in the observational case. Since the entanglement axes can transfer between the two setups, C_i and C_j cannot be disentangled, and therefore their minimal causal variables. \square

In other words, if two variables are always jointly intervened or passively observed, we cannot distinguish whether information belongs to causal variable C_i or C_j . Since the causal system is stationary, having one time step t for which $I_i^t \neq I_j^t$ implies that in the sample limit, we will observe samples with $I_i^t \neq I_j^t$ in the limit as well. Further, when we only observe joint interventions on two variables, C_i, C_j , the causal graph among the two variable cannot be identified for arbitrary distributions (Eberhardt, 2007), making the identifiability of the graph and variables impossible.

CITRIS (Lippe et al., 2022b) additionally requires that two intervention targets cannot be the invert of each other, i.e. $I_i^t = 1 - I_j^t$. However, this is not strictly required here, since for $I_i^t = 1$, the perfect interventions imply C_i being independent of all its parents, which is not the case for the observational regime, i.e. $I_i^t = 0$. Thus, as long as C_i and C_j have any parents, there is a possibility to disambiguate the variables even under $\forall t, I_i^t = 1 - I_j^t$.

Still, since there may exist variables without parents, we take the same assumption as Lippe et al. (2022b). Specifically, for every causal variable C_i with observed interventions, we require that the

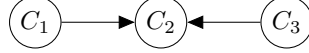


Figure 5: Example instantaneous causal graph between 3 causal variables C_1, C_2, C_3 . Without temporal dependencies, we could encode information of C_1 dependent on C_3 without needing an edge in the distribution.

following independence holds:

$$C_i^{t+1} \perp\!\!\!\perp I_i^{t+1} | C^t, \text{pa}^{t+1}(C_i^{t+1}), I_j^{t+1} \text{ for any } i \neq j \quad (19)$$

This also implies that there does not exist a variable C_j for which $\forall t, I_i^t = 1 - I_j^t$. As mentioned before, under additional assumptions such that every causal variable has at least one parents, it can be relaxed to unique interventions.

C.2.4 Assumption 4: The observational and interventional distributions share the same support

If the observational and interventional distribution do not share the same support, there exist data points for which the intervention targets can be determined from the observation X^t alone. In such situation, the encoder can change its encoding depending on the intervention target, as long as the decoder can yet recover the full observation. This can potentially create representation models that ignore the latent structure, since the intervention targets are already known. Furthermore, when intervention targets are known from seeing causal variables, we potentially introduce new independencies from intervention targets. For instance, if we have the graph $C_1, C_2 \rightarrow C_3$ where $I_3 = 1$ only if $I_1 = 1, I_2 = 0$, we can induce the intervention targets from other causal factors, making C_3 essential independent of I_3 . To prevent such degenerate solutions, we take the assumption that the observational and intervention distributions share the same support. This assumption implies that any data point could come from either the interventional or observational regime, ensuring that the intervention target cannot deterministically be found from an observation X^t .

C.2.5 Assumption 5: Temporal connections and interventions break all symmetries in the distributions

The temporal and interventional dependencies are an essential part in iCITRIS to guarantee identifiability and disentanglement of the causal variables. Without any of these dependencies, there may exist multiple representations that model the same distribution $p(X^t | X^{t-1}, I^t)$, while following the enforced latent structure by iCITRIS. The problem is that variables can functional dependent on each other, where these dependencies exploit symmetries, leaving the distribution unchanged.

For instance, consider the instantaneous causal graph of three variables C_1, C_2, C_3 with $C_1, C_3 \rightarrow C_2$, as depicted in Figure 5. Suppose that C_1 does not have any temporal parents, and the observational distribution of it follows a Gaussian: $p(C_1^t | I_1^t = 0) = \mathcal{N}(C_1^t | \mu_1, \sigma_1^2)$ with μ_1, σ_1^2 being constants. Further, suppose that under interventions, only the standard deviation changes, i.e. $p(C_1^t | I_1^t = 1) = \mathcal{N}(C_1^t | \mu_1, \tilde{\sigma}_1^2)$ with $\tilde{\sigma}_1^2 \neq \sigma_1^2$. Then, for any point $C_1^t = c_1$, there exists a second point, $c_1' = 2\mu_1 - c_1$, which has the same probability for any value of I_1^t . This is because both distributions, $p(C_1^t | I_1^t = 0)$ and $p(C_1^t | I_1^t = 1)$, share a symmetry around the mean μ_1 .

Now, suppose we have the optimal encoder which maps an observation X^t of this system to the three causal variables with their ground truth values. Then, there exist an alternative encoder, which flips the observed value of C_1^t around the mean μ_1 , deterministically conditioned on the remaining variables C_2^t and C_3^t . For instance, we could have the following representation $\hat{C}_1^t, \hat{C}_2^t, \hat{C}_3^t$ for the causal variables:

$$\hat{C}_2^t = C_2^t, \hat{C}_3^t = C_3^t, \hat{C}_1^t = \begin{cases} C_1^t & \text{if } \hat{C}_3^t > 0 \\ 2\mu_1 - C_1^t & \text{otherwise} \end{cases} \quad (20)$$

This alternative representation model shares the same likelihood as the optimal encoder in terms of $p(X^t | X^{t-1}, I^t)$, since flipping the value of C_1^t around the mean does not change its probability. Further, despite the flipping, the original observation X^t can be recovered from this alternative representation \hat{C}^t by the decoder, because the possible conditioning factors, i.e. \hat{C}_3^t in this case, are observable to the decoder. Hence, both representations are equally valid for the causal models. Yet,

one cannot recover the value of the true causal variable, C_1^t , from its alternative representation \hat{C}_1^t alone, since \hat{C}_3^t needs to be known to invert the example condition. This shows that we can have functional dependencies between representations of causal variables while their distributions remain independent. Thus, there exist more than one representation that cannot be distinguished between from having samples of $p(X^t|X^{t-1}, I^t)$ alone.

More generally speaking, functional dependencies between variables can be introduced if there exists a transformation that leaves the probability of a variable C_i unchanged for any possible value of its parents unseen in X^t , i.e. its intervention target I_i^t and temporal parents C^{t-1} . Whether this transformation is performed or not can now be conditioned on other variables at time step t . Meanwhile, this transformation does not introduce additional dependencies in the causal graph, since the distribution does not change.

To prevent such transformations from being possible, the temporal parents and intervention targets need to break all symmetries in the distributions. We can specify it in the following assumption:

Assumption 5: For a causal variable C_i and its causal mechanism $p(C_i^t|pa^{t+1}(C_i), pa^t(C_i), I_i^t)$, there exist no invertible, smooth transformation T with $T(C_i^t|C_{-i}^t) = \tilde{C}_i^t$ besides the identity, for which the following holds:

$$\forall C^{t-1}, C^t, I^t : p(C_i^t|pa^{t+1}(C_i^t), pa^t(C_i^t), I_i^t) = \left| \frac{\partial T(C_i^t|C_{-i}^t)}{\partial C_i^t} \right| \cdot p(\tilde{C}_i^t|pa^{t+1}(C_i^t), pa^t(C_i^t), I_i^t) \quad (21)$$

Intuitively, this means that there does not exist any symmetry that is shared across all possible values of the parents (temporal and interventions) of a causal variable. While this might first sound restricting, this assumption will likely hold in most practical scenarios. For instance, if the distribution is a Gaussian, then the assumption holds as long as the mean is not constant since the intervention breaks any parent dependencies are broken by the perfect interventions. The same holds in higher dimensions, as the new symmetries, i.e. rotations, are yet broken if the center point is not constant. Note that these symmetries can be smooth transformations, in contrast to the discontinuous flipping operation on the Gaussian (i.e. either we flip the distribution or not, but there is no step in between).

C.2.6 Assumption 6: Causal graph structure requirements

Besides disentangling and identifying the true causal variables, we are also interested in finding the instantaneous causal graph. This requires us to perform causal discovery, for which we need to take additional assumptions. First, we assume that the causal graph is acyclic, i.e. for any causal variable C_i^t , there does not exist a path through the directed causal graph that loops back to it. Note that this excludes different instances over time, meaning that a path from C_i^t to $C_i^{t+\tau}$ is not considered a loop. In real-world setups, there potentially exist instantaneous graphs which are not acyclic, which essentially model a feedback loop over multiple variables. However, to rely on the graph as a distribution factorization, we assume it to be acyclic, and leave extension to cyclic causal graphs for future work. As the second causal graph assumption, we require that the causal graph is faithful, which means that all independences between causal variables are implications of the graph structure, not the specific parameterization of the distributions (Hyttinen et al., 2013; Pearl, 2009). Without faithfulness, the graph might not be fully recoverable. Finally, we assume causal sufficiency, i.e. there do not exist any additional latent confounders that introduce dependencies between variables beyond the ones we model. Note that this excludes the potential latent confounder between the intervention targets, and we rather focus on confounders on the causal variables C_1, \dots, C_K besides their intervention targets, the previous time step C^t , and instantaneous parents C^{t+1} .

C.3 Theorem 3.2 - Proof outline

The goal of this section is to proof Theorem 3.2: the global optimum of iCITRIS will identify the minimal causal variables and their instantaneous causal graph. The proof follows a similar structure as Lippe et al. (2022b) used for proving the identifiability in CITRIS, but requires additional steps to integrate the possible instantaneous relations. In summary, we will take the following steps in the proof:

1. (Appendix C.4) Firstly, we show that the function δ^* that disentangles the true latent variables

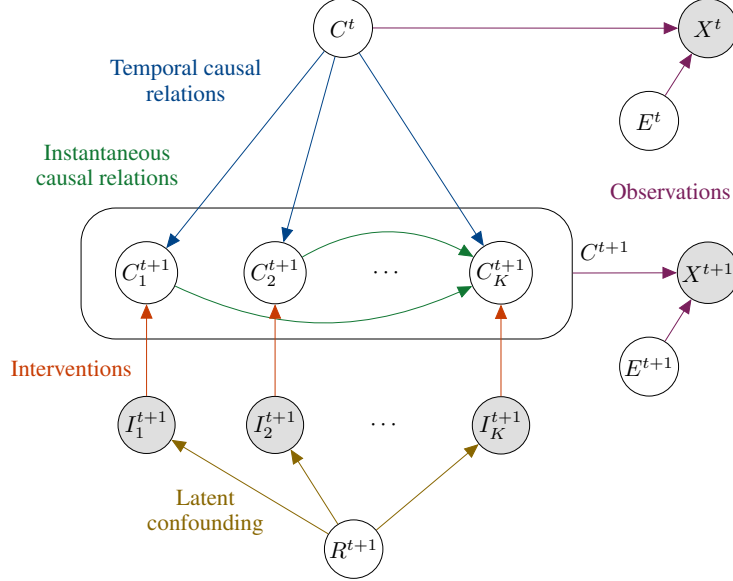


Figure 6: An example causal graph in iTRIS. A latent causal factor C_i^{t+1} can have as potential parents the causal factors at the **previous time step** $C^t = (C_1^t, \dots, C_K^t)$, **instantaneous parents** $C_j^{t+1}, i \neq j$, and its **intervention target** I_i^{t+1} . All causal variables C^{t+1} and the noise E^{t+1} cause the **observation** X^{t+1} . R^{t+1} is a potential **latent confounder** between the intervention targets.

- C_1, \dots, C_K and assigns them to the corresponding sets $z_{\psi_1}, \dots, z_{\psi_K}$ constitutes a global, but not necessarily unique, optimum for maximizing the likelihood $p(X^{t+1}|X^t, I^{t+1})$.
2. (Appendix C.5) Next, we characterize the class of disentanglement functions Δ^* which all represent a global maximum of the likelihood, *i.e.* get the same score as the true disentanglement. We do this by proving that all functions in Δ^* must disentangle the minimal causal variables.
 3. (Appendix C.6) In a third step, we show that based on the disentanglement of the minimal causal variables, the causal graph on these learned representations must contain at least the same edges as in the ground truth graph.
 4. (Appendix C.7) Finally, we put all parts together and derive Theorem 3.2.

We will make use of Figure 6 summarizing the temporal causal graph, and the notation introduced in Appendix C.1. For the remainder of the proof, we assume for simplicity of exposition that:

- The invertible map g_θ and the prior $p_\phi(z^{t+1}|z^t, I^{t+1})$ are sufficiently complex to approximate any possible function and distribution one might consider in iTRIS. In practice, over-parameterized neural networks can approximate most functions with sufficient accuracy.
- The latent dimension size is unlimited, *i.e.* $Z \in \mathbb{R}^\infty$. This is assumed such that there are no limitations on how many latent variables z_{ψ_i} can be used to represent a causal factor C_i . To maintain invertibility in g_θ , we assume that dimensions beyond $\dim(\mathcal{C}) + \dim(\mathcal{E})$ can potentially become constants. In practice, however, this is not a limiting factor as long as we can overestimate the dimensions of the causal factors and noise variables.
- The sample size for the provided experimental settings is unlimited. This ensures that dependencies and conditional independencies in the causal graph of Figure 6 transfer to the observed dataset, and no additional relations are introduced by sample biases. In practice, a large sample size is likely to give an accurate enough description of the true distributions.

C.4 Theorem 3.2 - Proof Step 1: The true model is a global optimum of the likelihood objective

We start the identifiability discussion by proving the following Lemma:

Lemma C.3. *The true disentanglement function δ^* that correctly disentangles the true causal factors $C_1^{t+1}, \dots, C_K^{t+1}$ from observations X^t, X^{t+1} using the true ψ^* assignment function on the latent variables Z^{t+1} and the true causal graph G^* is one of the global maxima of the likelihood of $p(X^{t+1}|X^t, I^{t+1})$.*

This lemma ensures that the true model is part of the solution space of maximum likelihood objective on $p(X^{t+1}|X^t, I^{t+1})$.

Proof. In order to prove this, we first rewrite the objective in terms of the true causal factors. This can be done by using the causal graph in Figure 6, which represents the true generative model:

$$p(X^t, X^{t+1}, C^t, C^{t+1}, I^{t+1}) = p(X^{t+1}|C^{t+1}) \cdot \left[\prod_{i=1}^K p(C_i^{t+1}|C^t, \text{pa}_G^{t+1}(C_i^{t+1}), I_i^{t+1}) \right] \cdot p(X^t|C^t) \cdot p(C^t) \cdot p(I^{t+1}) \quad (22)$$

The context variable R^{t+1} is subsumed in $p(I^{t+1})$, since it is a confounder between the intervention targets and is independent of all other factors given I^{t+1} .

In order to obtain $p(X^{t+1}|X^t, I^{t+1})$ from $p(X^t, X^{t+1}, C^t, C^{t+1}, I^{t+1})$, we need to marginalize out C^t and C^{t+1} , and condition the distribution on X^t and I^{t+1} :

$$p(X^{t+1}|X^t, I^{t+1}) = \int_{C^{t+1}} \int_{C^t} p(X^{t+1}|C^{t+1}) \cdot \left[\prod_{i=1}^K p(C_i^{t+1}|C^t, \text{pa}_G^{t+1}(C_i^{t+1}), I_i^{t+1}) \right] \cdot p(C^t|X^t) dC^t dC^{t+1} \quad (23)$$

In the assumptions with respect to the observation function h , we have defined h to be bijective, meaning that there exists an inverse f that can identify the causal factors C^t and noise variable E^t from X^t . The noise variables thereby represent all the stochasticity in the observation function that is not described by the causal factors. For instance, this can be color shifts, limited observation noise, or similar. However, independent of the noise, the causal factors need to be identifiable. This means that the joint dimensionality of the noise and the causal factor are limited by the image size: $\dim(\mathcal{C}) + \dim(\mathcal{E}) \leq \dim(\mathcal{X})$. The observation function h can represent an invertible map between the two spaces even under $\dim(\mathcal{C}) + \dim(\mathcal{E}) < \dim(\mathcal{X})$, since \mathcal{X} does not necessarily need to be $\mathbb{R}^{\dim(\mathcal{X})}$, but rather a subspace.

Using the invertible map, we can write $p(C^t|X^t) = \delta_{f(X^t)=C^t}$, where δ is a Dirac delta. We also remove E^t from the conditioning set since it is independent of X^{t+1} . This leads us to:

$$p(X^{t+1}|X^t, I^{t+1}) = \int_{C^{t+1}} \left[\prod_{i=1}^K p(C_i^{t+1}|C^t, \text{pa}_G^{t+1}(C_i^{t+1}), I_i^{t+1}, I_i^{t+1}) \right] \cdot p(X^{t+1}|C^{t+1}) dC^{t+1} \quad (24)$$

We can use a similar step to relate X^{t+1} with C^{t+1} and E^{t+1} . However, since we model a distribution over X^{t+1} , we need to respect possible non-volume preserving transformations. Hence, we use the change of variables formula with the Jacobian $J_h = \frac{\partial h(C^{t+1}, E^{t+1})}{\partial C^{t+1} \partial E^{t+1}}$ of the observation function h to obtain:

$$p(X^{t+1}|X^t, I^{t+1}) = |J_h|^{-1} \cdot \left[\prod_{i=1}^K p(C_i^{t+1}|C^t, \text{pa}_G^{t+1}(C_i^{t+1}), I_i^{t+1}) \right] \cdot p(E^{t+1}) \quad (25)$$

Since Equation (25) is a derivation of the true generative model $p(X^t, X^{t+1}, C^t, C^{t+1}, I^{t+1})$, it constitutes a global optimum of the maximum likelihood. Hence, one cannot achieve higher likelihoods by reparameterizing the causal factors or having a different graph, as long as the graph is directed and acyclic.

In the next step, we relate this maximum likelihood solution to iCITRIS, more specifically, the prior of iCITRIS. For this setting, the learnable, invertible map g_θ is identical to the inverse of the observation function, h^{-1} . In terms of the latent variable prior, we have defined our objective of iCITRIS as:

$$p_\phi(z^{t+1}|z^t, I^{t+1}) = \prod_{i=0}^K p_\phi(z_{\psi_i}^{t+1}|z^t, z_{\psi_i^{\text{pa}}}^{t+1}, I_i^{t+1}) \quad (26)$$

Since we know that g_θ^* is an invertible function between \mathcal{X} and \mathcal{Z} , we know that z^t must include all information of X^t . Thus, we can also replace it with $z^t = [C^t, E^t]$, giving us:

$$p_\phi(z^{t+1}|C^t, E^t, I^{t+1}) = \prod_{i=0}^K p_\phi(z_{\psi_i^*}^{t+1}|C^t, E^t, z_{\psi_i^{\text{pa}}}^{t+1}, I_i^{t+1}) \quad (27)$$

Next, we consider the assignment function ψ^* . The optimal assignment function ψ^* assigns sufficient dimensions to each causal factor C_1, \dots, C_K , such that we can consider $z_{\psi_i^*}^{t+1} = C_i^{t+1}$ for $i = 1, \dots, K$. Further, the same graph G is used in the latent space as in the ground truth, except that we additionally condition $z_{\psi_i^*}, i = 1, \dots, K$ on $z_{\psi_0^*}$. With that, Equation (27) becomes:

$$p_\phi(z^{t+1}|C^t, E^t, I^{t+1}) = \left[\prod_{i=1}^K p_\phi(z_{\psi_i^*}^{t+1} = C_i^{t+1}|C^t, z_{\psi_i^{\text{pa}}}^{t+1}, z_{\psi_0^*}^{t+1}, I_i^{t+1}) \right] \cdot p(z_{\psi_0^*}^{t+1}|C^t, E^t) \quad (28)$$

where we remove E^t from the conditioning set for the causal factors, since know that C^{t+1} and E^{t+1} is independent of E^t . Now, $z_{\psi_0^*}$ must summarize all information of z^{t+1} which is not modeled in the causal graph. Thus, $z_{\psi_0^*}$ represents the noise variables: $z_{\psi_0^*}^{t+1} = E^{t+1}$.

$$p_\phi(z^{t+1}|C^t, E^t, I^{t+1}) = \left[\prod_{i=1}^K p_\phi(z_{\psi_i^*}^{t+1} = C_i^{t+1}|C^t, z_{\psi_i^{\text{pa}}}^{t+1}, z_{\psi_0^*}^{t+1}, I_i^{t+1}) \right] \cdot p(z_{\psi_0^*}^{t+1} = E^{t+1}|C^t, E^t) \quad (29)$$

Finally, by using g_θ^* , we can replace the distribution on z^{t+1} by a distribution on X^{t+1} by the change of variables formula:

$$p_\phi(X^{t+1}|C^t, E^t, I^{t+1}) = \left| \frac{\partial g_\theta^*(z^{t+1})}{\partial z^{t+1}} \right| \cdot \left[\prod_{i=1}^K p_\phi(z_{\psi_i^*}^{t+1} = C_i^{t+1}|C^t, z_{\psi_i^{\text{pa}}}^{t+1}, z_{\psi_0^*}^{t+1}, I_i^{t+1}) \right] \cdot p(z_{\psi_0^*}^{t+1} = E^{t+1}|C^t, E^t) \quad (30)$$

We can simplify this distribution by using the independencies of the noise term E^{t+1} in the causal graph of Figure 6:

$$p_\phi(X^{t+1}|C^t, E^t, I^{t+1}) = \left| \frac{\partial g_\theta^*(z^{t+1})}{\partial z^{t+1}} \right| \cdot \left[\prod_{i=1}^K p_\phi(z_{\psi_i^*}^{t+1} = C_i^{t+1}|C^t, z_{\psi_i^{\text{pa}}}^{t+1}, I_i^{t+1}) \right] \cdot p(z_{\psi_0^*}^{t+1} = E^{t+1}) \quad (31)$$

With this, Equation (31) represents the exact same distribution as Equation (25). Therefore, we have shown that the function δ^* that disentangles the true latent variables C_1, \dots, C_K and assigns them to the corresponding sets $z_{\psi_1}, \dots, z_{\psi_K}$ constitutes a global optimum for maximizing the likelihood. However, this solution is not necessarily unique, and additional optima may exist. In the next steps of the proof, we will discuss the class of disentanglement functions and graphs that lead to the same optimum. \square

C.5 Theorem 3.2 - Proof Step 2: Characterizing the disentanglement class

In this section, we discuss the disentanglement and identifiability results of the causal variables in iCITRIS. We first describe the minimal causal variables in iTRIS, and how they differ to TRIS in CITRIS (Lippe et al., 2022b). Next, we identify the information that must be assigned to individual parts of the latent representation, and similarly, what needs to be disentangled. Finally, we discuss the final setup to ensure disentanglement, including the additional variables in z_{ψ_0} .

C.5.1 Minimal causal variables

Lippe et al. (2022b) introduced the concept of a minimal causal variable as an invertible split of a causal variable C_i into one part that is strictly dependent on the intervention, $s^{\text{var}}(C_i)$, and a part that is independent of it, $s^{\text{inv}}(C_i)$. For iCITRIS, we consider the same concept, but adapt it to the setup of iTRIS.

First, iTRIS assumes the presence of perfect interventions. When given perfect interventions, we

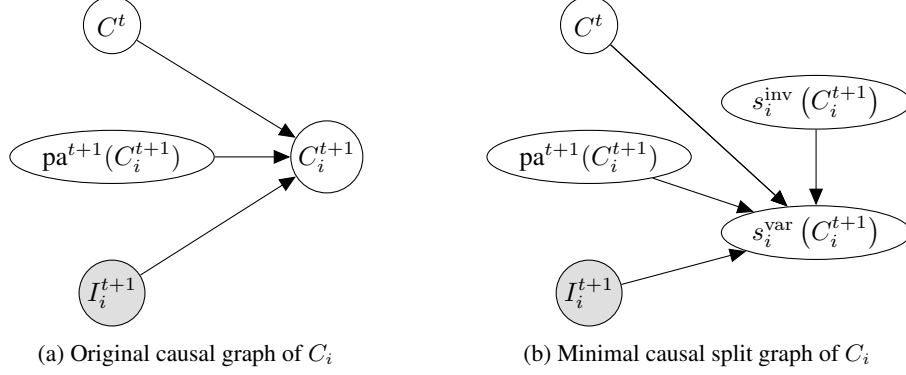


Figure 7: The minimal causal variable in terms of a causal graph under iTRIS. (a) In the original causal graph, C_i^{t+1} has as potential parents the causal variables of the previous time step C^t (eventually a subset), its instantaneous parents $\text{pa}^{t+1}(C_i^{t+1})$, and the intervention target I_i^{t+1} . (b) The minimal causal variable splits C_i^{t+1} into an invariable part $s_i^{\text{inv}}(C_i^{t+1})$ and variable part $s_i^{\text{var}}(C_i^{t+1})$. The invariable part $s_i^{\text{inv}}(C_i^{t+1})$ is independent of *all* parents due to perfect interventions. However, it can be a parent of $s_i^{\text{var}}(C_i^{t+1})$ due to the autoregressive distribution modeling.

can ensure that $s_i^{\text{inv}}(C_i)$ does not have any parents. This is because under interventions, a causal variable C_i becomes independent of all its parents, and hence $s_i^{\text{inv}}(C_i)$ must be as well. Since $s_i^{\text{inv}}(C_i)$ is independent of I_i and thus does not change its mechanism with the intervention, $s_i^{\text{inv}}(C_i)$ must *always* be independent of all parents of C_i . Hence, we can limit our discussion to splits where $s_i^{\text{inv}}(C_i)$ does not have any parents.

Second, the presence of a causal graph in iCITRIS allows dependencies between different parts of the latent space. Further, z_{ψ_0} can be the parent of any other set of variables, thus allowing for potential dependencies between $s_i^{\text{inv}}(C_i)$ and $s_i^{\text{var}}(C_i)$. Note that those, however, must also be cut off by the perfect intervention. Hence, the split $s_i(C_i^t) = (s_i^{\text{var}}(C_i^t), s_i^{\text{inv}}(C_i^t))$ must have the following distribution structure:

$$p(s_i(C_i^{t+1})|C^t, \text{pa}^{t+1}(C_i^{t+1}), I_i^{t+1}) = p(s_i^{\text{var}}(C_i^{t+1})|C^t, \text{pa}^{t+1}(C_i^{t+1}), s_i^{\text{inv}}(C_i^{t+1}), I_i^{t+1}) \cdot p(s_i^{\text{inv}}(C_i^{t+1})) \quad (32)$$

where

$$p(s_i^{\text{var}}(C_i^{t+1})|C^t, \text{pa}^{t+1}(C_i^{t+1}), s_i^{\text{inv}}(C_i^{t+1}), I_i^{t+1}) = \begin{cases} \tilde{p}(s_i^{\text{var}}(C_i^{t+1})) & \text{if } I_i^{t+1} = 1 \\ p(s_i^{\text{var}}(C_i^{t+1})|C^t, \text{pa}^{t+1}(C_i^{t+1}), s_i^{\text{inv}}(C_i^{t+1})) & \text{otherwise} \end{cases} \quad (33)$$

Thereby, the minimal causal variable with respect to its intervention variable I_i^{t+1} is the split s_i which maximizes the information content $H(s_i^{\text{inv}}(C_i^t))$. These relations are visualized in Figure 7.

Causal variables for which the intervention target is constant, i.e. no interventions have been observed, were modeled by $s_i^{\text{inv}}(C_i) = C_i, s_i^{\text{var}}(C_i) = \emptyset$ in CITRIS (Lippe et al., 2022b). Here, this does not naturally hold anymore since $s_i^{\text{inv}}(C_i)$ is restricted to not having any parents. Hence, for the simplicity of exposition in this proof, we add the exception that for a causal variable C_i , if $I_i^t = 0$ for all t , its minimal causal split is defined as $s_i^{\text{inv}}(C_i) = C_i, s_i^{\text{var}}(C_i) = \emptyset$.

C.5.2 Identifying the minimal causal variables

As a first step towards disentanglement, we postulate the following lemma:

Lemma C.4. *For all representation functions in the disentanglement class Δ^* , there exist a deterministic map from the latent representation z_{ψ_i} to the minimal causal variable $s_i^{\text{var}}(C_i)$ for all causal variables $C_i, i = 1, \dots, K$.*

This lemma intuitively states that the minimal causal variable $s_i^{\text{var}}(C_i)$ is modeled in the latent

representation z_{ψ_i} for any representation that maximizes the likelihood objective. Note that this does not imply exclusive modeling yet, meaning that z_{ψ_i} can contain more information than just $s^{\text{var}}(C_i)$. We will discuss this aspect in Appendix C.5.3.

Proof. In order to prove this lemma, we first review some relations between the conditional and joint entropy. Consider two random variables A, B of arbitrary space and dimension. The conditional entropy between these two random variables is defined as $H(A|B) = H(A, B) - H(B)$ (Cover and Thomas, 2005). Further, the maximum of the joint entropy is the sum of the individual entropy terms, $H(A, B) \leq H(A) + H(B)$ (Cover and Thomas, 2005). Hence, we get that $H(A|B) = H(A, B) - H(B) \leq H(A) + H(B) - H(B) = H(A)$. In other words, the entropy of a random variable A can only become lower when conditioned on any other random variable B .

Using this relation, we move now to identifying the minimal causal variables. If a minimal causal variable is the empty set, i.e. $s^{\text{var}}(C_i) = \emptyset$, for instance due to not having observed interventions on C_i , the lemma is already true by construction since no information must be modeled in z_{ψ_i} . Thus, we can focus on cases where $s^{\text{var}}(C_i) \neq \emptyset$, which implies that $C_i^{t+1} \not\perp I_i^{t+1}$. Therefore, the following inequality must strictly hold:

$$H(C_i^{t+1}|C^t, C_{-i}^{t+1}) < H(C_i^{t+1}|C^t, C_{-i}^{t+1}, I_i^{t+1}) \quad (34)$$

for all $i = 1, \dots, K$. Additionally, based on the assumption that the observational and interventional distributions share the same support, we know that the intervention posterior, i.e. $p(I^{t+1}|X^{t+1})$, cannot be deterministic for any data point X^{t+1} and intervention target I_i^{t+1} . Thus, we cannot derive I_i^{t+1} from the observation X^{t+1} . Thirdly, because every latent variable is only conditioned on exactly one intervention target in iCITRIS and there exist no deterministic function between any pair of intervention targets, one cannot identify I_i^{t+1} in any latent variables except z_{ψ_i} . Therefore, the only way in iCITRIS to fully exploit the information of the intervention target I_i^{t+1} is to model its dependent information in z_{ψ_i} . As this information corresponds to the minimal causal variable, $s^{\text{var}}(C_i)$, any representation function must model the distribution $p(s^{\text{var}}(C_i)|\dots)$ in $p(z_{\psi_i}|I_i^{t+1}, \dots)$ to achieve the maximum likelihood solution. This is independent of the modeled causal graph structure, meaning that if there exist representation functions with different graphs in Δ^* , then all of them must model $s^{\text{var}}(C_i)$ in z_{ψ_i} . Finally, using assumption 5 (Appendix C.2.5), we obtain that this distributional relation implies a functional independence of $s^{\text{var}}(C_i)$ in z_{ψ_i} to any other latent variable. Thus, there exists a deterministic map from z_{ψ_i} to $s^{\text{var}}(C_i)$ in any of the maximum likelihood solutions. \square

C.5.3 Disentangling the minimal causal variables

The previous subsection showed that z_{ψ_i} models the minimal causal variable $s^{\text{var}}(C_i)$. This, however, is not necessarily the only information in z_{ψ_i} . For instance, for two random variables $A, B \in \mathbb{R}$, the following distributions are identical:

$$p(A) \cdot p(B|A) = p(A) \cdot p(B + A|A) = p(A) \cdot p(B, A|A) \quad (35)$$

The second distribution can add additional information about A arbitrarily to B without changing the likelihoods. This is because the distribution is conditioned on A , and the conditional entropy of a random variable to itself is $H(A|A) = H(A) - H(A) = 0$. Hence, for arbitrary autoregressive distributions, we cannot disentangle variables from each other purely by looking at the likelihoods.

However, in iTRIS, we are given perfect interventions under which variables are strictly independent of their parents. With this, we postulate the following lemma:

Lemma C.5. *For all representation functions in the disentanglement class Δ^* , z_{ψ_i} does not contain information about any other minimal causal variable $s^{\text{var}}(C_j), j \neq i$, except $s^{\text{var}}(C_i)$, i.e. $H(z_{\psi_i}|s^{\text{var}}(C_i)) = H(z_{\psi_i}|s^{\text{var}}(C_i), s^{\text{var}}(C_j))$.*

Proof. In order to prove this lemma, we consider all augmented graph structures that are induced by the provided perfect interventions. Specifically, given a graph $G = (V, E)$ with V being its vertices and E its edges, and a set of binary intervention targets $I = \{I_1, \dots, I_{|V|}\}$, we construct an augmented DAG $G' = (V', E')$, where $V' = V$ and $E' = E \setminus \{\{\text{pa}_G(V_i) \rightarrow V_i\} | i = 1, \dots, |V|, I_i = 1\}$. In other words, the augmented graph G' has all its input edges to intervened variables removed. An example for a graph of three variables and its three single-target interventions is shown in Figure 8.

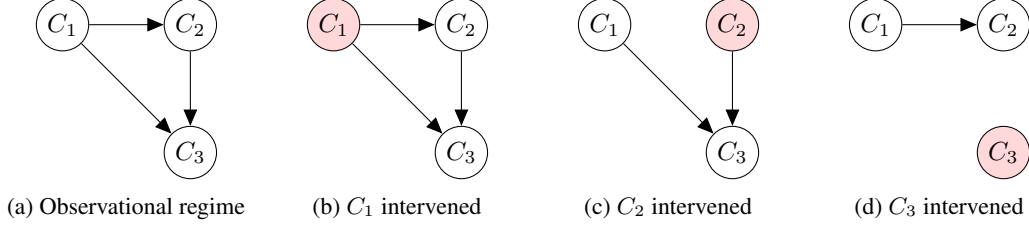


Figure 8: Example instantaneous causal graph between 3 causal variables C_1, C_2, C_3 , and the augmented graphs under different perfect, single-target interventions. The augmented graphs have the edges to the intervened variables removed. For readability, the intervened variables are colored in red in the graphs.

A representation function in the disentanglement class Δ^* must model the optimal likelihood for *all* intervention-augmented graphs of its originally learned graph \hat{G} , since it cannot achieve lower likelihood for any of the graphs than the ground truth. For every pair of variables C_i, C_j , assumption 3 (Appendix C.2.3) ensures that there exist one out of three possible experiment sets: (1) we observe $I_i^t = 1, I_j^t = 0$ and $I_i^t = 0, I_j^t = 1$, (2) $I_i^t = 0, I_j^t = 0, I_i^t = 1, I_j^t = 0$, and $I_i^t = 1, I_j^t = 1$, or (3) $I_i^t = 0, I_j^t = 0, I_i^t = 0, I_j^t = 1$, and $I_i^t = 1, I_j^t = 1$. In all cases, there exist at least one augmented graph in which $z_{\psi_i} \perp\!\!\!\perp z_{\psi_j}$ since (2) and (3) observe joint interventions on both variables. In (1), a constant connection between the two variables would require both edges $C_i \rightarrow C_j$ and $C_j \rightarrow C_i$ in the graph which is not acyclic. Under the augmented graph, where $z_{\psi_i} \perp\!\!\!\perp z_{\psi_j}$, the optimal likelihood can only be achieved if z_{ψ_i} is actually independent of z_{ψ_j} , thus not containing any information about $s^{\text{var}}(C_j)$. The same holds for z_{ψ_j} . Hence, a representation function in the disentanglement class Δ^* must disentangle the minimal causal variables in the latent space. \square

C.5.4 Disentangling the remaining variables

In Appendix C.5.2 and Appendix C.5.3, we have shown that for any solution in the disentanglement class Δ^* , we can ensure that z_{ψ_i} models the minimal causal variable $s^{\text{var}}(C_i)$, and none other. Still, there exist more dimensions that need to be modeled. The causal variables without interventions, the invariant parts of the causal variables, $s^{\text{inv}}(C_i)$, as well as the noise variables E^t are part of the generative model that influence an observation X^t . All these variables share the property that they are not instantaneous children of any minimal causal variable, and can only be parents of them. This leads to the situation that any of these variables could be modeled in the latent representation of z_{ψ_i} for an arbitrary $i = 1, \dots, K$ as long as C_i is the parent of the same variables. The reason for this is that the distribution modeling of such variables is independent of interventions.

To exclude them from the causal variable modeling, we follow the same strategy as in CITRIS (Lippe et al., 2022b) by taking the representation function that maximizes the entropy of z_{ψ_0} :

Lemma C.6. *For all representation functions in the disentanglement class Δ^* that maximize the entropy of $p(z_{\psi_0}|C^t)$, the latent representation z_{ψ_i} models exclusively the minimal causal variable $s^{\text{var}}(C_i)$ for all causal variables $C_i, i = 1, \dots, K$.*

Proof. Using Lemma C.4 and Lemma C.5, we know that the only remaining information besides the minimal causal variables are the causal variables without interventions, invariant parts of the causal variables, $s^{\text{inv}}(C_i)$, as well as the noise variables E^t . All these variables cannot be children of the observed, intervened variables, as the assumption 2 (Appendix C.2.2) states. Thus, the remaining information $\mathcal{M} = \{s^{\text{inv}}(C_1), \dots, s^{\text{inv}}(C_K), E^t\}$ can be optimally modeled by $p(\mathcal{M}|z^t)p(z_{\psi_1}, \dots, z_{\psi_K}|\mathcal{M}, z^t, I^{t+1})$. This implies that there exist a solution where $z_{\psi_0} = \mathcal{M}$, which can be found by searching for the solution with the maximum entropy of $p(z_{\psi_0}|C^t)$. In this solution, the latent representation $z_{\psi_1}, \dots, z_{\psi_K}$ does not model any subset of \mathcal{M} , hence modeling the minimal causal variables exclusively. \square

The overall disentanglement result is that we identify the minimal causal variables in $z_{\psi_1}, \dots, z_{\psi_K}$, and all remaining information is modeled in z_{ψ_0} . Note that the causal variables without interventions, the noise variables and the invariant part of the causal variables can be arbitrarily entangled in z_{ψ_0} . Furthermore, since there exist variables in z_{ψ_0} that may not have any temporal parents (e.g. the noise

variables and invariable parts of the intervened causal variables), we cannot rely on assumption 5 (Appendix C.2.5) to ensure functional independence. Hence, while the distribution of $p(z_{\psi_0}|z^t)$ is independent of $z_{\psi_1}, \dots, z_{\psi_K}$, there may exist dependencies such that for a single data point, a change in z_{ψ_i} can result in a change of the noise or invariable parts of the causal variables in the observational space.

C.6 Theorem 3.2 - Proof Step 3: Identifiability of the causal graph

In this step of the proof, we discuss the identifiability of the causal graph under the findings of the disentanglement. In the first subsection, we discuss what graph we can optimally find under the disentanglement of the minimal causal variables. In the second part, we then show how the maximum likelihood objective is sufficient for identifying the instantaneous causal graph. Finally, we discuss the identifiability of the temporal causal graph.

C.6.1 Causal graph on minimal causal variables

The identification of the causal graph naturally depends on the learned latent representations of the causal variables. In Appendix C.5, we have shown that one can only guarantee to find the minimal causal variables in iTRIS. Thus, we are limited to finding the causal graph on the minimal causal variables $s^{\text{var}}(C_1), s^{\text{var}}(C_2), \dots, s^{\text{var}}(C_K)$ and the additional variables modeled in z_{ψ_0} . The graph between the minimal causal variables is not necessarily equal to the ground truth graph. For instance, consider a 2-dimensional position (x, y) and the color of an object as two causal variables. If the x -position causes the color, but the minimal causal variable of the position is only $s^{\text{var}}(C_1) = y$, then the color has only $s^{\text{inv}}(C_1)$ as parent, not $s^{\text{var}}(C_1)$. In the learned graph on the latent representation, it would mean that we do not have an edge between z_{ψ_1} and z_{ψ_2} , but instead $z_{\psi_0} \rightarrow z_{\psi_2}$. Hence, we might have a mismatch between the ground truth graph on the full causal variables, and the graph on the modeled minimal causal variables.

Still, there are patterns and guarantees that one can give for how the optimal, learned graph looks like. Due to the interventions being perfect, the invariable part of a causal variable, $s^{\text{inv}}(C_i)$, cannot have any parents. Thus, the parents of a minimal causal variable $s^{\text{var}}(C_i)$ are the same ground truth causal variables as in the true graph, i.e. $\text{pa}(C_i) = \text{pa}(s^{\text{var}}(C_i))$. The difference is how the parents are represented. Since each parent $C_j \in \text{pa}(C_i)$ is split into a variable and invariable part, any combination of the two can represent a parent of $s^{\text{var}}(C_i)$. Thus, the learned set of parents for $s^{\text{var}}(C_i)$, i.e. $\text{pa}(z_{\psi_i})$, must be a subset of $\{s^{\text{var}}(C_j) | C_j \in \text{pa}(C_i)\} \cup \{z_{\psi_0}\}$. This implies that if there is no causal edge between two causal variables C_i and C_j in the ground truth causal graph, then there is also no edge between their minimal causal variables $s^{\text{var}}(C_i)$ and $s^{\text{var}}(C_j)$. The causal graph between the true variables and the minimal causal variables therefore shares a lot of similarities, and in practice, is often almost the same.

The additional latent variables z_{ψ_0} summarize all invariable parts of the intervened variables, the remaining causal variables without interventions, and the noise variables. Therefore, z_{ψ_0} cannot be an instantaneous child of any minimal causal variable, and we can predefine the orientation for those edges in the instantaneous graph.

Next, we can discuss the identifiability guarantees for the graph on the minimal causal variables. For simplicity, in the rest of the section, we refer to identifying the causal graph on the minimal causal variables as identifying the graph on C_1, \dots, C_K .

C.6.2 Optimizing the maximum likelihood objective uniquely identifies the causal graph under perfect interventions

Several causal discovery works have shown before that causal graphs can be identified when given sufficient interventions (Brouillard et al., 2020; Eberhardt, 2007; Lippe et al., 2022a; Pearl, 2009). Since the disentanglement of the causal variables already requires perfect interventions, we can exploit these interventions for learning and identifying the graph as well. In assumption 6 (Appendix C.2.6), we have assumed that the causal graph to identify is faithful. This implies that any dependency between two variables, C_1, C_2 , which have a causal relation among them ($C_1 \rightarrow C_2$ or $C_2 \rightarrow C_1$), cannot be replaced by conditioning C_1 and/or C_2 on other variables. In other words, in order to optimize the overall likelihood $p(C_1, \dots, C_K)$, we require a graph that has a causal edge between two variables if they are causally related. Now, we are interested in whether we can identify the

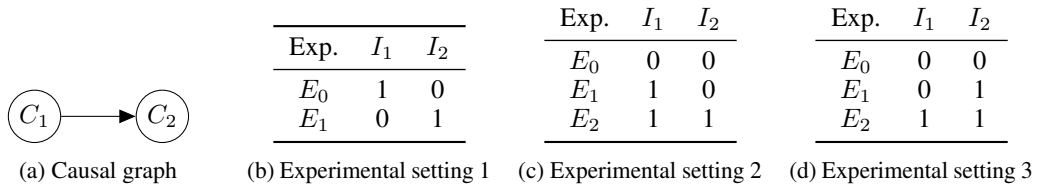


Figure 9: Identifiability of a causal relation between two variables C_1, C_2 under different interventional settings. (a) The causal relation to consider. The discussion is identical in case of the reverse orientation by switching the variable names C_1 and C_2 . (b-d) The tables describe the minimal sets of experiments, i.e. unique combinations of I_1, I_2 in the dataset, that guarantee the intervention targets to be unique, i.e. not $\forall t, I_1^t = I_2^t$. Under each of these sets of experiments, we show that the maximum likelihood solution of $p(C_1, C_2 | I_1, I_2)$ uniquely identifies the causal orientation.

Table 3: The probability distribution $p(C_1, C_2 | I_1, I_2)$ for all possible causal graphs among the two causal variables C_1, C_2 under different experimental settings. Observational distributions are denoted with $p(\dots)$, and interventional with $\tilde{p}(\dots)$. Note that under interventions, it is enforced that $\tilde{p}(\dots)$ is not conditioned on any parents, since we assume perfect interventions.

Interventions		Causal graph		
I_1	I_2	$C_1 \rightarrow C_2$	$C_2 \rightarrow C_1$	$C_1 \perp\!\!\!\perp C_2$
0	0	$p(C_1)p(C_2 C_1)$	$p(C_2)p(C_1 C_2)$	$p(C_1)p(C_2)$
1	0	$\tilde{p}(C_1)p(C_2 C_1)$	$p(C_2)\tilde{p}(C_1)$	$\tilde{p}(C_1)p(C_2)$
0	1	$p(C_1)\tilde{p}(C_2)$	$\tilde{p}(C_2)p(C_1 C_2)$	$p(C_1)\tilde{p}(C_2)$
1	1	$\tilde{p}(C_1)\tilde{p}(C_2)$	$\tilde{p}(C_1)\tilde{p}(C_2)$	$\tilde{p}(C_1)\tilde{p}(C_2)$

orientation between every pair of causal variables that have a causal relation in the ground truth graph, which leads us to the following lemma:

Lemma C.7. *In iTRIS, the orientation of an instantaneous causal effect between two causal variables C_i, C_j can be identified by solely optimizing the likelihood of $p(C_i, C_j | I_i, I_j)$.*

Proof. To discuss the identifiability of the causal direction between two variables C_1, C_2 , we need to consider all possible minimal sets of experiments that fulfill the intervention setup in assumption 3 (Appendix C.2.3). These three sets are shown in Figure 9. For all three sets, we have to show that the maximum likelihood of the conditional distribution $p(C_1, C_2 | I_1, I_2)$ can only be achieved by modeling the correct orientation, here $C_1 \rightarrow C_2$. For cases where the true graph is $C_2 \rightarrow C_1$, the same argumentation holds, just with the variables names C_1 and C_2 swapped. As an overview, Table 3 shows the distribution $p(C_1, C_2 | I_1, I_2)$ under all possible experiments and causal graphs.

Experimental setting 1 (Figure 9b) In the first experimental setting, we are given single target interventions on C_1 and C_2 . In the experiment E_0 which represents interventions on C_1 and passive observations on C_2 , the dependency between C_1 and C_2 persists in the ground truth, i.e. $C_1 \not\perp\!\!\!\perp C_2 | I_1 = 1, I_2 = 0$. Hence, only causal graphs that condition C_2 on C_1 under interventions on C_1 can achieve the maximum likelihood in E_0 . From Table 3, we see that the only causal graph that does this is $C_1 \rightarrow C_2$. Thus, when single-target interventions on C_1 are observed, we can uniquely identify the orientation of its outgoing edges.

Experimental setting 2 (Figure 9c) The second experimental setting provides the observational regime (E_0), interventions on C_1 with C_2 being passively observed (E_1), and joint interventions on C_1 and C_2 (E_2). Since the experiment E_1 gives us the same setup as in experimental setting 1, we can directly conclude that the causal orientation $C_1 \rightarrow C_2$ is yet again identifiable.

Experimental setting 3 (Figure 9d) In the final experimental setting, C_1 is only observed to be jointly intervened upon with C_2 , not allowing for the same argument as in the experimental settings 1 and 2. However, the causal graph yet remains identifiable because of the following reasons. Firstly, the experiment E_0 with its purely observational regime cannot be optimally modeled by a causal graph without an edge between C_1 and C_2 , reducing the set of possible causal graph to $C_1 \rightarrow C_2$ and $C_2 \rightarrow C_1$. Under the joint interventions E_2 , both causal graphs model the same distribution.

Still, under the experiment E_1 where only C_2 has been intervened upon, the two distributions differ. The graph with the anti-causal orientation compared to the true graph, $C_2 \rightarrow C_1$, uses the same distribution as in the observational regime to model C_1 , i.e. $p(C_1|C_2)$. In order for this to achieve the same likelihood as the true orientation, it would need to be conditioned on I_2 as the following derivation from the true distribution $p(C_1, C_2|I_1, I_2)$ shows:

$$p(C_1, C_2|I_1, I_2) = p(C_2|I_1, I_2) \cdot p(C_1|C_2, I_1, I_2) \quad (36)$$

$$p(C_1|C_2, I_1, I_2) = \begin{cases} p(C_1|I_1) & \text{if } I_2 = 1 \\ p(C_1|C_2, I_1) & \text{if } I_2 = 0 \end{cases} \quad (37)$$

This derivation shows that $p(C_1|C_2, I_1, I_2)$ strictly depends on I_2 if $p(C_1|C_2, I_1, I_2 = 1) \neq p(C_1|C_2, I_1, I_2 = 0)$, which is ensured by C_1, C_2 not being conditionally independent in the ground truth graph. As the causal graph $C_2 \rightarrow C_1$ models C_1 independently of I_2 , it therefore cannot achieve the maximum likelihood solution in this experimental settings. Hence, the only graph achieving the maximum likelihood solution is $C_1 \rightarrow C_2$, such that the orientation can again be uniquely identified.

All other, possible experimental settings must contain one of the three previously discussed experiments as a subset, due to assumption 3 (Appendix C.2.3). Hence, we have shown that for all valid experimental settings, optimizing the maximum likelihood objective uniquely identifies the causal orientations between pairs of variables under perfect interventions. \square

Based on these orientations, we can exclude all additional edges that could introduce a cycle in the graph, since we strictly require an acyclic graph. The only remaining non-identified parts of the graph are edges among variables that are independent, conditioned on their parents. In terms of maximum likelihood, these edges do not influence the objective since for two variables C_1, C_2 with $C_1 \perp\!\!\!\perp C_2$, $p(C_1) \cdot p(C_2) = p(C_1|C_2) \cdot p(C_2) = p(C_1) \cdot p(C_2|C_1)$. Hence, the equivalence class in terms of maximum likelihood includes all graphs that at least contain the true edges, and are acyclic. By requiring structural minimality, i.e. taking the graph with the least amount of edges that yet fully describe the probability distribution, we can therefore identify the full causal graph between C_1, \dots, C_K .

C.6.3 Identifying the temporal causal relations by pruning edges

So far, we have shown that the instantaneous causal relations can be identified between the minimal causal variables. Besides the instantaneous graph, there also exist temporal relations between C^t and C^{t+1} , which we also aim to identify:

Lemma C.8. *In iTRIS, the temporal causal graph between the minimal causal variables can be identified by removing the edge between any pair of variables $z_{\psi_i}^t, z_{\psi_j}^{t+1}$ with $i, j \in \llbracket 0..K \rrbracket$, if $z_{\psi_i}^t \perp\!\!\!\perp z_{\psi_j}^{t+1} | z_{\psi_{-i}}^t, \text{pa}^{t+1}(z_{\psi_j}^{t+1})$.*

Proof. The prior in Equation (1) conditions the latent variables z^{t+1} on all variables of the previous time step, z^t . Thus, this corresponds to modeling a fully connected graph from $z_{\psi_0}^t, z_{\psi_1}^t, \dots, z_{\psi_K}^t$ to $z_{\psi_0}^{t+1}, z_{\psi_1}^{t+1}, \dots, z_{\psi_K}^{t+1}$. Since any temporal edge must be oriented from z^t to z^{t+1} , it is clear that the true temporal graph, G_T , must be a subset of this graph. Further, since in assumption 6 (Appendix C.2.6), we have stated that the true causal model is faithful, we know that two variables, $z_{\psi_i}^t$ and $z_{\psi_j}^{t+1}$, are only connected by an edge, if they are not conditionally independent of each other: $z_{\psi_i}^t \not\perp\!\!\!\perp z_{\psi_j}^{t+1} | z_{\psi_{-i}}^t, \text{pa}^{t+1}(z_{\psi_j}^{t+1})$. This implies that all redundant edges must be between two, conditionally independent variables with: $z_{\psi_i}^t \perp\!\!\!\perp z_{\psi_j}^{t+1} | \text{pa}^t(z_{\psi_j}^{t+1}), \text{pa}^{t+1}(z_{\psi_j}^{t+1})$ with $\text{pa}^t(z_{\psi_j}^{t+1})$ being a subset of $z_{\psi_{-i}}^t$. Thus, we can find the true temporal graph by iterating through all pairs of variables $z_{\psi_i}^t$ and $z_{\psi_j}^{t+1}$, and remove the edge if both of them are conditionally independent given $z_{\psi_{-i}}^t, \text{pa}^{t+1}(z_{\psi_j}^{t+1})$. \square

C.7 Theorem 3.2 - Proof Step 4: Final identifiability result

Using the results derived in Appendix C.4, Appendix C.5 and Appendix C.6, we are finally able to derive the full identifiability results. In Appendix C.5, we have shown that any solution that maximizes the likelihood $p_{\phi, \theta, G}(x^{t+1} | x^t, I^{t+1})$ disentangles the minimal causal variables of C_1, \dots, C_K in

$z_{\psi_1}, \dots, z_{\psi_K}$. Further, we are able to summarize all remaining variables in z_{ψ_0} by maximizing the entropy (LDDP) of $p_\phi(z_{\psi_0}^{t+1}|z^t)$. In Appendix C.6, we have used this disentanglement condition to show that the causal graph that maximizes the likelihood must have at least the same edges as the ground truth graph on the minimal causal variables. To obtain the full ground truth graph, we need to pick the one with the least edges.

These aspects together can be summarized into the following theorem:

Theorem C.9. *Suppose that ϕ^* , θ^* , ψ^* and G^* are the parameters that, under the constraint of maximizing the likelihood $p_{\phi, \theta, G}(x^{t+1}|x^t, I^{t+1})$, maximize the information content of $p_\phi(z_{\psi_0}^{t+1}|z^t)$ and minimize the number of edges in G^* . Then, with sufficient latent dimensions, the model ϕ^*, θ^*, ψ^* learns a latent structure where $z_{\psi_i}^{t+1}$ models the minimal causal variable of C_i , and G^* is the true instantaneous causal graph between these minimal causal variables. Further, pruning edges between time steps t and $t+1$ identifies the true temporal graph. Finally, z_{ψ_0} models all remaining information.*

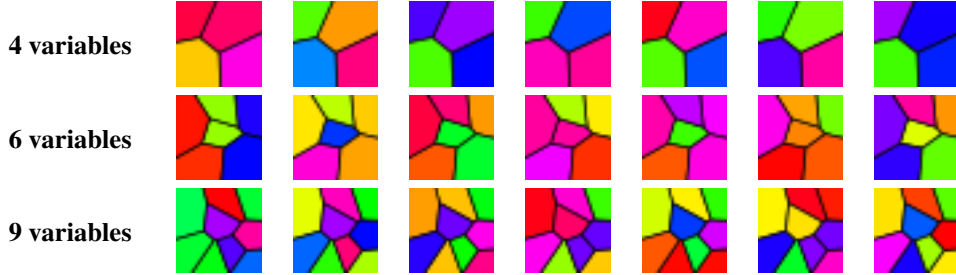


Figure 10: Example sequences of the Voronoi benchmark for the different graph sizes. Each image of 32×32 is partitioned into K patches. The values of the K true causal variables have been transformed by a two-layer normalizing flow, which result into the hues of the K patches in $[-\frac{7}{8}\pi, \frac{7}{8}\pi]$. The hues are finally mapped into the RGB space, resulting in the images above.

D Datasets

The following section gives a detailed overview of the dataset and used hyperparameters in all settings. Appendix D.1 contains the description of the Voronoi benchmark, for which the experimental results are shown in Section 5.2. Appendix D.2 discusses the Instantaneous Temporal Causal3DIdent dataset, and Appendix D.3 the Causal Pinball dataset.

D.1 Voronoi benchmark

The purpose of the Voronoi benchmark is to provide a flexible, synthetic dataset where we can evaluate causal representation learning models on various settings, such as number of variables and graph structure (both instantaneous and temporal). For each dataset, we generate one sequence with 150k time steps, in between which single-target interventions may have been performed. We sample the interventions with $1/(K+2)$ for each variable, and with $2/(K+2)$ a purely observational regime. A visual example of the Voronoi benchmark is shown in Figure 10, and we describe its generation steps below.

D.1.1 Network setup

In the Voronoi benchmark, we need a data generation mechanism for the conditional distributions $p(C_i^{t+1} | \text{pa}(C_i^{t+1}))$ that support any set of parents. For this, we deploy randomly initialized neural networks which models arbitrary, non-linear relations between any parent set and a causal variable. We visualize the network architecture in Figure 11. As a simplified setup, we use the neural networks to parameterize a Gaussian distribution. Specifically, the neural networks take as input a subset of C^t, C^{t+1} according to the given graph structure (see next subsection for the graph generation), and output a scalar representing the mean of the conditional distribution $\mathcal{N}(C_i^{t+1} | \mu(\text{pa}(C_i^{t+1})), \sigma^2)$ where the standard deviation is set to $\sigma = 0.3$. We have also experimented with having the (log) standard deviation as an additional output of the network. However, we experienced that this leads to the true causal variables to be the optimal solution when modeling K conditionally independent factors. Hence, both iCITRIS and the baselines were able to identify the causal variables well, making the task easier than anticipated. The interventional distribution is thereby set to $\mathcal{N}(0, 1)$ for all causal variables.

On the causal variables, we apply a normalizing flow which consisted of six layers: Activation Normalization, Autoregressive Affine Coupling, Activation Normalization, Invertible 1x1 convolution, Autoregressive Affine Coupling, Activation Normalization. The Activation Normalization (Kingma and Dhariwal, 2018) layers are initialized once after the Batch Normalizations of the distribution neural networks have been set, and ensure that all outputs roughly have a zero mean and standard deviation of one. The Autoregressive Affine Coupling layers use randomly initialized neural networks, with the average standard deviation of the outputs being 0.2. The coupling layer is volume preserving, *i.e.* we do not use a scaling term in the affine coupling, to prevent any issues with the image quantization. The Invertible 1x1 convolution (Kingma and Dhariwal, 2018) is initialized with a random, orthogonal matrix, entangling all causal variables across dimensions. Hence, each output of the normalizing flow is influenced by all causal variables.

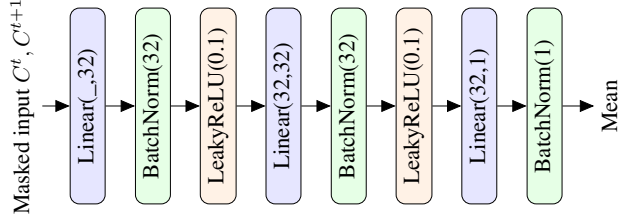


Figure 11: Network architecture of the randomly initialized neural networks in the Voronoi benchmark, modeling the conditional distributions $p(C_i^{t+1} | \text{pa}(C_i^{t+1}), I_i^{t+1} = 0) = \mathcal{N}(C_i^{t+1} | \mu(\text{pa}(C_i^{t+1})), \sigma^2)$ with $\sigma = 0.3$. The BatchNorm layers (Ioffe and Szegedy, 2015) are initialized by sequentially sampling 100 batches of the causal variables, using each as the input to the next batch. This ensures that the marginal distribution $p(C_i^{t+1})$ has a mean close to zero and standard deviation of one.

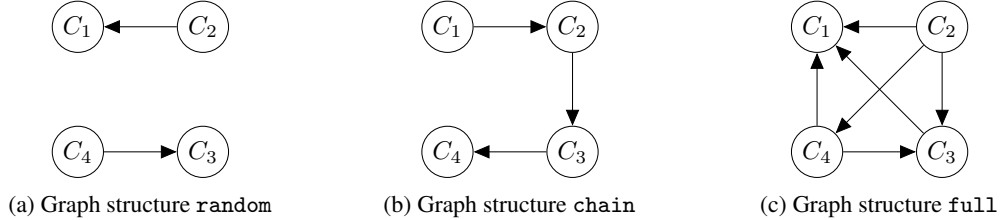


Figure 12: Example instantaneous causal graphs with four variables for the three graph structures. The causal ordering for the causal variables is randomly sampled for each graph to prevent any structural biases.

Finally, the outputs of the normalizing flow are transformed by the function $f(x) = \frac{7}{8}\pi \cdot \tanh\left(\frac{x}{2}\right)$. This function maps all values to a range of $[-\frac{7}{8}\pi, \frac{7}{8}\pi]$, which we can use as hues in the patches of the Voronoi diagram. The division by 2 of x is performed to reduce the number of data points in the saturation points of the \tanh . The Voronoi diagrams are generated by sampling K points on the image, which have a distance of at least 5 pixels between each other, and are fixed within a dataset. In contrast to just mapping the colors into a grid, the Voronoi diagram is an irregular structure. Hence, the mapping from images to the K color is non-trivial and does not transfer across datasets. Once the Voronoi diagram was created, we have used matplotlib (Hunter, 2007) to visualize the structure as an RGB image.

D.1.2 Graph generations

For the instantaneous causal graph, we have considered three graph structures: random, chain, and full. An example of each is visualized in Figure 12.

The random graph samples an edge for every possible pair of variables $C_i, C_j, i \neq j$ with a chance of 0.5. Thereby, we ensure that the graph is acyclic by sampling undirected edges, and directing them according to a randomly sampled ordering of the variables. This way, the average number of edges in the graph is $\frac{K(K-1)}{4}$. For small graphs of size 4, this results in variables to eventually having no incoming or outgoing edges, testing also the model’s ability on conditionally independent variables.

The chain graph connects the variables in a sequence, where each variable is the parent of the next one in the sequence. This leads to each graph having $K - 1$ edges, *i.e.* the sparsest, yet continuously connected graph.

The full graph represents the densest directed acyclic graph possible. We first sample an ordering of variables, and then add an edge from each variable to all others that follow it in the sequence. Thus, it has the most possible edges in a DAG, namely $\frac{K(K-1)}{2}$.

Finally, the temporal graph is sampled similar to the random graph. However, the orientations are pre-determined by the temporal ordering, and no cycles can occur. We therefore sample a directed edge between any pair of variables C_i^t, C_j^{t+1} , including $i = j$, with a chance of 0.25. This leads to an



Figure 13: Example sequence from the training set of the Instantaneous Temporal Causal3DIdent dataset (from left to right, top to bottom). Each image is of size 64×64 pixels. One can see the instantaneous effects of the background influencing the object color, for instance, or the object color again influencing the rotation of the object.

average number of edges of $\frac{K^2}{4}$. Additionally, we ensure that every variable has at least one temporal parent, to prevent variance collapses in the neural network distributions.

D.2 Instantaneous Temporal Causal3DIdent

The creation of the Instantaneous Temporal Causal3DIdent dataset closely followed the setup of von Kügelgen et al. (2021); Lippe et al. (2022b), and we show an example sequence of the dataset in Figure 13. We used the code provided by Zimmermann et al. (2021)² to render the images via Blender (Blender Online Community, 2021), and used the following seven object shapes: Cow (Crane, 2021), Head (Rusinkiewicz et al., 2021), Dragon (Curless and Levoy, 1996), Hare (Turk and Levoy, 1994), Armadillo (Krishnamurthy and Levoy, 1996), Horse (Praun et al., 2000), Teapot (Newell, 1975). As a short recap, the seven causal factors are: the object position as multidimensional vector $[x, y, z] \in [-2, 2]^3$; the object rotation with two dimensions $[\alpha, \beta] \in [0, 2\pi]^2$; the hue of the object, background and spotlight in $[0, 2\pi)$; the spotlight’s rotation in $[0, 2\pi)$; and the object shape (categorical with seven values). We refer to Lippe et al. (2022b, Appendix C.1) for the full detailed dataset description of Temporal Causal3DIdent, and describe here the steps taken to adapt the datasets towards instantaneous effects.

The original temporal causal graph of the Temporal Causal3DIdent dataset contains 15 edges, of which 8 are between different variables over time. Those relations form an acyclic graph, which we can directly move to instantaneous relations. Thus, the adjacency matrix of the temporal graph is an identity matrix, while the instantaneous causal graph is visualized in Figure 14. The causal mechanisms remain unchanged, except that the inputs may now be instantaneous. For instance, the spotlight rotation is adapted as follows:

$$\text{Previous version: } \text{rot_s}^{t+1} = f(\text{atan2}(\text{pos_x}^t, \text{pos_y}^t), \text{rot_s}^t, \epsilon_{rs}^t) \quad (38)$$

$$\text{Instantaneous version: } \text{rot_s}^{t+1} = f(\text{atan2}(\text{pos_x}^{t+1}, \text{pos_y}^{t+1}), \text{rot_s}^t, \epsilon_{rs}^t) \quad (39)$$

where $f(a, b, c) = \frac{a-b}{2} + c$. The causal parents of other variables, here pos_x and pos_y , are now instantaneous instead of the previous time step. Hence, an intervention on the position will lead to an instantaneous effect on the rotation of the spotlight. All remaining aspects of the dataset generation are identical to the Temporal Causal3DIdent dataset.

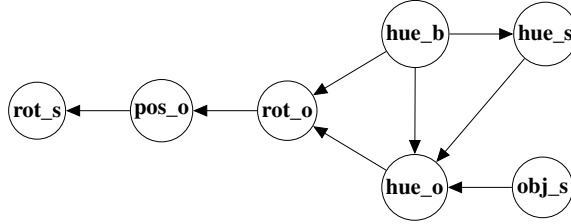


Figure 14: The instantaneous causal graph in the Instantaneous Temporal Causal3DIdent dataset. The graph contains several common sub-structures, such as a chain ($\text{rot}_o \rightarrow \text{pos}_o \rightarrow \text{rot}_s$), a fork ($\text{hue}_o, \text{hue}_b \rightarrow \text{rot}_o$), and confounders ($\text{hue}_b \rightarrow \text{hue}_s, \text{hue}_o$). The most difficult edges to recover include $\text{rot}_o \rightarrow \text{pos}_o$ since the object orientation has a complex, non-linear relation to the observation space which is difficult to model and prone to noise. Further, the edge $\text{hue}_b, \text{hue}_s \rightarrow \text{hue}_o$ only holds for two object shapes (Hare and Dragon), for which the background and spotlight hue have an influence on the object color. For the other five object shapes, the object color is independent of the other two parents.

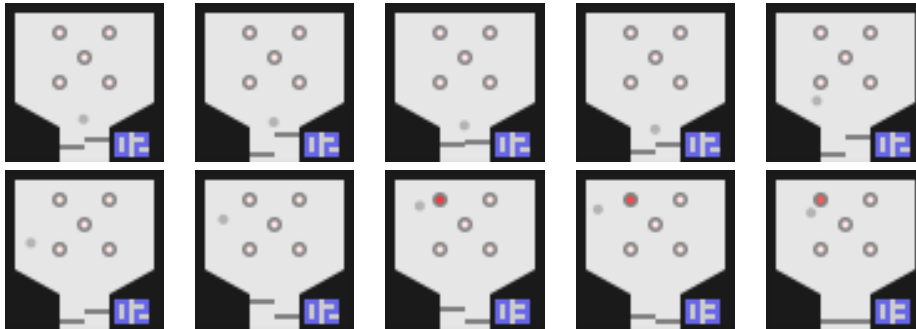


Figure 15: An example sequence of the Pinball dataset, from left to right, top to bottom. The paddles, *i.e.* the two gray rectangles in the bottom center, are accelerated forwards under interventions such that they make a large jump within an image. For instance, in image 5, the right paddle has been intervened upon and hits the ball (gray circle). It is accelerated immediately, showcasing the instantaneous effect between the two. When no interventions on the paddles are given, they slowly move backwards. In image 8, the ball hits a bumper (5 circle centers with light red filling) which lights up. This represents the scoring of a point, as the instantaneous increase in points shows in image 8 (the digits in the bottom right corner). Note that technically, there is no winning or losing state here since we do not focus on learning a policy, but instead a causal representation of the components. Further, not shown here, there exist a fourth channel representing the ball’s velocity.

D.3 Causal Pinball

The Causal Pinball dataset is a simplified environment of the popular game Pinball, as shown in Figure 15. In Pinball, the user controls two fixed paddles on the bottom of the playing field, and tries to hit the ball such that it collides with various objects for scoring points. There are several versions of Pinball, but for this dataset, we limit it to the essential parts representing the five, multidimensional causal variables:

- The **ball** is defined by four dimensions: the position on the x- and y-axis, and its velocity in x and y. Both are continuous values, with the position being limited to the available spots on the field.
- The **left paddle y-position** (`paddle_left`) describes the position of the left paddle. Its maximum is close-to the top of the black border next to it (*e.g.* image 7 in Figure 15), and its minimum is close to the bottom (*e.g.* image 10 in Figure 15).
- The **right paddle y-position** (`paddle_right`) is similar to `paddle_left`, just for the right paddle.
- The **bumpers** represent the activation, *i.e.* the light, of all 5 bumpers. It is a five-dimensional

²<https://github.com/brendel-group/cl-ica>

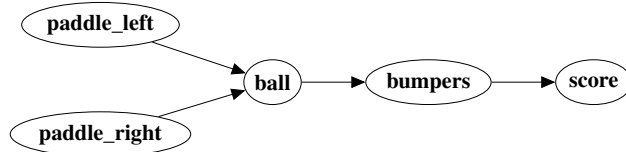


Figure 16: The instantaneous causal graph in the Causal Pinball dataset. An intervention on the paddles can have an immediate effect on the ball by changing its position and velocity. A change in the ball’s position again influences the bumpers, whether their light is activated or not. Finally, when the bumpers are activated, the score increases in the same time step.

continuous variable, each dimension being between 0 (light off, *e.g.* image 1 in Figure 15) and 1 (light fully on, *e.g.* image 8 in Figure 15).

- The **score** is a categorical variable summarizing the number of points the player has scored. Its value ranges from 0 to a maximum of 20.

The dynamics between these causal factors resembles the standard game dynamics of Pinball, which results in the instantaneous causal graph in Figure 16. The ball can collide with the paddles, borders, and bumpers. When it collides with the borders, it is simply reflected, and we reduce its velocity by 10% (*i.e.* multiply by 0.9). Under collisions with the paddles, we distinguish between a collision where the paddle has been static or moving backwards, versus a collision where the paddle was moving. When the paddle was static, we use the same collision dynamics as the borders, except that we reduce its y -velocity by 70% to reduce oscillations around the paddle position. When the paddle was moving, we instead set the y -velocity of the ball to the y -velocity of the paddle. Finally, when the ball collides with a bumper, it activates the bumper’s light and reflects from it, similar to the borders. When a bumper’s light is turned on, we increase the score by one, but include a 5% chance that the score is not increased to introduce some stochastic elements and faulty components in the game. Next to the collisions, the ball is influenced by a gravity towards the bottom, adding a constant every time step to its y -velocity, and friction that reduces its velocity by 2% after each time step.

In terms of interventions, we sample the interventions on the five elements independently, but with a chance that would correspond more closely to the game dynamics. Specifically, we intervene on the paddles in 20% of the frames, 10% on the ball, and 5% each the score and bumpers. An intervention of the paddle represents it moving forwards, from its previous position, to a randomly sampled position between the middle and maximum paddle position. Its velocity is set to the difference between the previous position and new position. Since these interventions are usually elements of the standard Pinball game play, we sample them rather often with 20%. An intervention on the ball represents moving it to a position between the two paddles and the bumpers, with a small velocity sampled randomly. In real-life, this would correspond to a player picking up the ball and placing it in a new position. An intervention on the bumpers is that we randomly set the bumper lights either to 0 or 1 with a 50% chance. Finally, an intervention on the score resets it to a random value between 0 and 4.

To render the images, we use matplotlib (Hunter, 2007) and a resolution of 64×64 pixels. The images are generated by having a single sequence of 150k images.

Algorithm 1 Pseudocode of the training algorithm for the prior and graph learning in iCITRIS with NOTEARS as graph learning method. For efficiency, all for-loops are processed in parallel in the code.

Require: batch of observation samples and intervention targets: $\mathcal{B} = \{x^t, x^{t+1}, I^{t+1}\}_{n=1}^N$

- 1: **for** each batch element x^t, x^{t+1}, I^{t+1} **do**
- 2: Encode observations into latent space: $z^t = g_\theta(x^t), z^{t+1} = g_\theta(x^{t+1})$
- 3: Differentiably sample one graphs G : $G_{ij} \sim \text{GumbelSoftmax}(1 - \sigma(\gamma_{ij}), \sigma(\gamma_{ij}))$
- 4: Sample latent to causal assignments from ψ for each batch element
- 5: **for** each causal variable C_i **do**
- 6: Determine parent mask from G : $S \in \{0, 1\}^M, S_j = G_{\psi(j), i}$
- 7: Calculate $\text{nll}_i = -\log p_\phi(z_{\psi_i}^{t+1} | z^t, z^{t+1} \odot S, I_i^{t+1})$
- 8: **end for**
- 9: Backpropagation loss $\mathcal{L}^n = \sum_{i=1}^K \text{nll}_i$
- 10: **end for**
- 11: Acyclicity regularizer: $\mathcal{L}^{\text{cycle}} = \text{tr}(\exp(\sigma(\gamma))) - K$
- 12: Sparsity regularizer: $\mathcal{L}^{\text{sparse}} = \frac{1}{K^2} \sum_{i=1}^K \sum_{j=1}^K \sigma(\gamma_{ij})$
- 13: Update parameters ϕ, ψ, γ with $\nabla_{\phi, \psi, \gamma} \left[\lambda_{\text{cycle}} \cdot \mathcal{L}^{\text{cycle}} + \lambda_{\text{sparse}} \cdot \mathcal{L}^{\text{sparse}} + \frac{1}{N} \sum_{n=1}^N \mathcal{L}^n \right]$

E Experimental details

In this section, we give further details on implementation details of iCITRIS and hyperparameters that were used for the experiments in Section 5.

E.1 iCITRIS - Model details

We discuss implementation details of the three main components of iCITRIS: the graph learning with NOTEARS, the graph learning with ENCO, and the mutual information estimator. For the two graph learning methods, we additionally discuss the setup used to learn the prior networks.

Graph Learning - NOTEARS The full training algorithm of iCITRIS with the NOTEARS graph parameterization is shown in Algorithm 1. The adjacency matrix is parameterized by $\gamma \in \mathbb{R}^{(K+1) \times (K+1)}$, where $\sigma(\gamma_{ij})$, with σ being the sigmoid function, represents the probability of having the edge $z_{\psi_i} \rightarrow z_{\psi_j}$ in the instantaneous graph. To prevent self-loops, we set $\gamma_{ii} = -\infty, i = 0, \dots, K$, and $\gamma_{i0} = -\infty, i = 1, \dots, K$ to guarantee an empty instantaneous parent set for z_{ψ_0} . At each training iteration, we sample an adjacency matrix per batch element using the Gumbel Softmax trick (Jang et al., 2017). These matrices are used to mask out the inputs to the prior, and therefore obtain gradients by optimizing the likelihood of the prior. Further, NOTEARS requires two regularizers. First, the acyclicity regularizer takes the matrix exponential of the edge probabilities, $\sigma(\gamma)$. The trace of this matrix exponential has a minimum of K , which is only achieved if the matrix does not contain any cycles. All operations in this regularizer are differentiable, and we weigh this regularizer in the loss by λ_{cycle} . This weighting factor follows a scheduling over training, which starts with a value of $\exp(-6) \approx 2.5e - 3$, and reaches a maximum of $\exp(4) \approx 54.6$. In our experiments, this maximum factor guaranteed the graph to be acyclic. Finally, the second regularizer is a sparsity regularizer, that removes redundant edges and is implemented as a L1 regularizer on the edge probabilities.

Graph Learning - ENCO The full training algorithm of iCITRIS with the ENCO graph parameterization is shown in Algorithm 2. The adjacency matrix is parameterized by two sets of parameters, with $\gamma \in \mathbb{R}^{(K+1) \times (K+1)}$ representing the edge existence parameters, and $\theta \in \mathbb{R}^{(K+1) \times (K+1)}$ the orientation parameters, with $\theta_{ij} = -\theta_{ji}$. The probability of an edge $z_{\psi_i} \rightarrow z_{\psi_j}$ in the instantaneous graph is determined by $\sigma(\gamma_{ij}) \cdot \sigma(\theta_{ij})$. Similar to NOTEARS, we prevent self-loops by setting $\gamma_{ii} = -\infty, i = 0, \dots, K$, and fix the orientations of the edges of z_{ψ_0} by setting $\theta_{i0} = -\theta_{0i} = -\infty, i = 1, \dots, K$. In contrast to NOTEARS, this parameterization leads to initial edge probabilities of 0.25. We found it beneficial to initialize the edge probabilities closer to 0.5, which we implement by initializing $\gamma_{ij} = 4, i \neq j, i, j \in \llbracket 1..K \rrbracket$ ($\sigma(4) \approx 0.98$). At each training iteration, we sample L graphs from ENCO. For all experiments, we found $L = 8$ to be sufficient. For each of these graphs, we evaluate the negative log likelihood of all variables. Note that in contrast to NOTEARS, this does not need to be differentiable with respect to γ and θ . Once all graphs are evaluated, we can determine

Algorithm 2 Pseudocode of the training algorithm for the prior and graph learning in iCITRIS with ENCO as graph learning method. For efficiency, all for-loops are processed in parallel in the code.

Require: batch of observation samples and intervention targets: $\mathcal{B} = \{x^t, x^{t+1}, I^{t+1}\}_{n=1}^N$

- 1: **for** each batch element x^t, x^{t+1}, I^{t+1} **do**
- 2: Encode observations into latent space: $z^t = g_\theta(x^t), z^{t+1} = g_\theta(x^{t+1})$
- 3: Sample L graphs G^1, \dots, G^L from $G_{ij}^l \sim \sigma(\theta_{ij})\sigma(\gamma_{ij})$
- 4: Sample latent to causal assignments from ψ for each batch element
- 5: **for** each graph G^l **do**
- 6: **for** each causal variable C_i **do**
- 7: Determine parent sets for graph G^l : $z_{\psi_i}^{t+1} = \{z_j^{t+1} | j \in \llbracket 1..M \rrbracket, \psi(j) \in \text{pa}_{G^l}(i)\}$
- 8: Calculate $\text{nll}_i^l = -\log p_\phi(z_{\psi_i}^{t+1} | z^t, z_{\psi_i}^{t+1}, I_i^{t+1})$
- 9: **end for**
- 10: **end for**
- 11: Backpropagation loss $\mathcal{L}^n = \frac{1}{L} \sum_{i=1}^K \sum_{l=1}^L \text{nll}_i^l$
- 12: Average nll for $C_i \rightarrow / \nrightarrow C_j$: $\text{pos_nll}_{ij}^n = \frac{\sum_{l=1}^L G_{ij}^l \text{nll}_i^l}{\sum_{l=1}^L G_{ij}^l}, \text{neg_nll}_{ij}^n = \frac{\sum_{l=1}^L (1 - G_{ij}^l) \text{nll}_i^l}{L - \sum_{l=1}^L G_{ij}^l}$
- 13: **end for**
- 14: Theta gradients: $\nabla(\theta_{ij}) = \sigma(\gamma_{ij})\sigma'(\theta_{ij}) \left(\frac{1}{N} \sum_{n=1}^N I_i^n (1 - I_j^n) (\text{pos_nll}_{ij}^n - \text{neg_nll}_{ij}^n) \right)$
- 15: Gamma gradients: $\nabla(\gamma_{ij}) = \sigma(\theta_{ij})\sigma'(\gamma_{ij}) \left(\frac{1}{N} \sum_{n=1}^N (1 - I_j^n) (\text{pos_nll}_{ij}^n - \text{neg_nll}_{ij}^n + \lambda_{\text{sparse}}) \right)$
- 16: Update theta and gamma with the gradients calculated above
- 17: Update distribution and assignment parameters ϕ, ψ with $\nabla_{\phi, \psi} \frac{1}{N} \sum_{n=1}^N \mathcal{L}^n$

the average negative log likelihood of a z_{ψ_j} under graphs with the edge $z_{\psi_i} \rightarrow z_{\psi_j}$, versus graphs where this edge was missing. We use this to determine the gradients of γ_{ij} and θ_{ij} , if z_{ψ_j} has not been intervened upon. For the gradients of θ_{ij} , we further mask out gradients for batch samples in which z_{ψ_i} has not been intervened upon. With these gradients, we can update the graph parameters, while the distribution parameters are updated based on the differentiable negative log likelihood. Note that the sparsity regularizer, λ_{sparse} , is integrated in the update of the γ parameters.

Prior networks Both graph learning algorithms use a prior network of the form $p_\phi(z_{\psi_i}^{t+1} | z^t, z_{\psi_i}^{t+1}, I_i^{t+1})$. To implement this efficiently in a neural network setting, we consider for each latent $z_m, m \in 1M$ a 2-layer neural network (hidden size 32 in all experiments), that take as input z^t, z^{t+1}, I^{t+1} , and a mask on z^{t+1} and I^{t+1} . Therefore, its input size is $M + M + K + M + K = 3M + 2K$. The mask on I^{t+1} depends on which causal variable the latent z_m has been assigned to, *i.e.* $z_{\psi_i}^{t+1}$ should only depend on I_i^{t+1} . The mask on z^{t+1} depends on the graph that was sampled, in combination with the causal variable assignment, *i.e.* only leave $z_{\psi_i}^{t+1}$ unmasked. Further, we can use an autoregressive prior over the potentially multiple dimensions of $z_{\psi_i}^{t+1}$ by leaving previous latents unmasked that have been assigned to the causal variable C_i . We use this autoregressive variant for the Instantaneous Temporal Causal3DIdent and Causal Pinball dataset, since the multiple dimensions in those causal factors may not be independent.

Mutual information estimator The full training algorithm of the mutual information estimator is shown in Algorithm 3. The MI estimator is a 2 layer network, that takes as input the latent parents of a causal variable, and its current value, and has a single output value. This value indicates whether the current causal variable and its parents match or not, *i.e.* is $z_{\psi_i}^{t+1}$ the value of C_i at time step $t + 1$ based on observing the parents z^t and $z_{\psi_i}^{t+1}$, or not. We train this network by a binary classification problem, where the model compares the true set of values, *i.e.* $z_{\psi_i}^{t+1}, z^t, z_{\psi_i}^{t+1}$, to a randomly picked time step $\tau, z_{\psi_i}^{\tau+1}, z^t, z_{\psi_i}^{\tau+1}$. Since the model does not have the precise time step t or τ as input, it has to deduce from the values of the causal variables whether they match or not. Under interventions, we know that for the true causal variables, the optimal performance of this binary classifier is 0.5, because C_i^{t+1} is independent of all its parents under perfect interventions. Thus, the gradients of the latents is to move the classifier closer to 0.5, which is equal to trying to increase the misclassification

Algorithm 3 Pseudocode of the training algorithm for the mutual information estimator in iCITRIS. For efficiency, all for-loops are processed in parallel in the code.

Require: batch of observation samples and intervention targets: $\mathcal{B} = \{x^t, x^{t+1}, I^{t+1}\}_{j=1}^N$

- 1: Encode all observations into latent space: $z^t = g_\theta(x^t), z^{t+1} = g_\theta(x^{t+1})$
- 2: Sample an instantaneous graph G from graph parameterization
- 3: Sample latent to causal assignments from ψ
- 4: **for** each causal variable C_i **do**
- 5: Filter out all batch elements for which $I_i^{t+1} = 0$
- 6: **for** each element in the filtered batch **do**
- 7: Determine parent sets for graph G : $z_{\psi_i^{\text{pa}}}^{t+1} = \{z_j^{t+1} | j \in \llbracket 1..M \rrbracket, \psi(j) \in \text{pa}_{G^t}(i)\}$
- 8: Calculate logits of positive pairs: $e_{\text{pos}} = \text{NN}_{\text{MI}}(z_{\psi_i}^{t+1}, z^t, z_{\psi_i^{\text{pa}}}^{t+1})$
- 9: For each batch element, sample a different, random time step in the batch, τ
- 10: Calculate logits of negative pairs: $e_{\text{neg}} = \text{NN}_{\text{MI}}(z_{\psi_i}^{\tau+1}, z^t, z_{\psi_i^{\text{pa}}}^{t+1})$
- 11: Calculate loss for MI estimator: $\mathcal{L}_i^{\text{NNMI}} = -e_{\text{pos}} + \log[\exp(e_{\text{pos}}) + \exp(e_{\text{neg}})]$
- 12: Calculate loss for latents: $\mathcal{L}_i^{\text{zMI}} = -e_{\text{neg}} + \log[\exp(e_{\text{pos}}) + \exp(e_{\text{neg}})]$
- 13: **end for**
- 14: **end for**
- 15: Update parameters of NN_{MI} according to avg loss $\mathcal{L}_i^{\text{NNMI}}$
- 16: Backpropagate gradients of latents according to avg loss $\mathcal{L}_i^{\text{zMI}}$

rate of the MI estimator. During training, we need to sample instantaneous graphs G from our graph parameterization. Since especially in the beginning, this graph is close to random, and the true causal variables still depend on their children, for instance, under interventions, it can lead to unstable behavior to train the MI estimator on all parents from the start. Thus, instead, we initially train the MI estimator with an empty instantaneous causal graph and try to make $z_{\psi_i}^{t+1}$ independent of z^t , *i.e.* its temporal parents. Over the progress of training, we introduce the instantaneous parents, similar to the graph learning scheduling, such that at the end of training, the MI estimator is fully trained on both temporal and instantaneous parents.

E.2 Hyperparameters

We have summarized an overview of all hyperparameters in Table 4. Additionally, we discuss the main hyperparameter choices for all models here.

Base VAE architecture For all VAE-based methods, we have applied the same VAE to have a fair comparison between methods. In particular, we have used a VAE with a normalizing flow prior (Rezende and Mohamed, 2015), inspired by the inverse autoregressive flows (Kingma et al., 2016). The encoder outputs the parameters for M independent Gaussian distributions. A sample of these Gaussians is used as input to the decoder to reconstruct the original image, but also as input to a four-layer autoregressive normalizing flow. This flow consists of a sequence of Activation Normalization (Kingma and Dhariwal, 2018), Invertible 1x1 Convolutions (Kingma and Dhariwal, 2018), and autoregressive affine coupling layers. The outputs of the flow are used as input to a prior, which is conditioned on the latents of the previous time step and the intervention targets. For iCITRIS, this prior follows the structure of Equation (1) including causal discovery. For CITRIS, this prior is similar to Equation (1), except that no instantaneous parents are modeled. For the iVAE, the prior is a 3-layer MLP that outputs M independent Gaussian distributions. Finally, for the iVAE-AR, the prior is a 2-layer autoregressive NN predicting N Gaussian distributions in sequence. The reconstruction loss is based on the Mean-Squared Error (MSE) objective, which provided much better results than learning a flexible distribution over the output images. The specific architecture of the encoder and decoder depends on the dataset, where we used simpler models where possible to reduce computational cost without losing significant performance. For the Voronoi benchmark, we use a 5-layer CNN. For the Instantaneous Temporal Causal3DIdent dataset and the Causal Pinball dataset, we used a 10-layer CNN for the encoder, and a 5-layer ResNet (He et al., 2016) as decoder.

Autoencoder + Normalizing flow architecture For iCITRIS and CITRIS, we use the variation of training a normalizing flow on a pretrained autoencoder for the Instantaneous Temporal Causal3DIdent and Causal Pinball dataset. The autoencoder uses the same encoder and decoder architecture as

the VAE, except that we increase the decoder size since it can be trained much faster than the VAE (does not require any temporal dimension), and, in contrast to the VAE, lead to improvements in the reconstruction for the two datasets. The autoencoder is trained on reconstructing the input images, where we add Gaussian noise with a small standard deviation (0.05) to the latents to simulate a distribution. Additionally, we apply a small L2 regularizer on the latents to prevent that the autoencoder counteracts the noise in the latents by artificially scaling up the standard deviation of the latents. For Causal3DIdent, we use a weight of $1e-5$ on this regularizer, and $1e-6$ for the Causal Pinball since its reconstructions obtain much lower losses. The normalizing flow, applied on it, follows the same architecture as in the VAE.

Optimizer For all models, we use the Adam optimizer (Kingma and Ba, 2015) with a learning rate of $1e-3$. Additionally, we warmup the learning rate for the first 100 steps. Afterwards, we follow a cosine annealing learning rate scheduling, that, over the course of the training, decreases the learning rate to $5e-5$.

Frameworks All models have been implemented and trained using PyTorch v1.10 (Paszke et al., 2019) and PyTorch Lightning v1.6.0 (Falcon and The PyTorch Lightning team, 2019).

E.3 Evaluation metrics

For the details on the correlation matrix evaluation, we refer to Lippe et al. (2022b, Appendix C.3.1). The causal graph evaluation is performed for each model in the same way. For each model, we use the checkpoint of the best training loss, and encode all observations to the latent space. Next, we need to separate the latent space into the causal variables. For iCITRIS and CITRIS, we use the learned assignment function ψ to assign latent variables to causal variables. Since the iVAE models do not learn such a latent-to-causal assignment, we instead assign each latent variable to the causal factor that it has the highest correlation to. This requires using the ground truth values of the causal variables, and hence gives the iVAE an advantage over iCITRIS and CITRIS. With this separation, we apply ENCO (Lippe et al., 2022a) to learn the temporal and instantaneous graph. Since iCITRIS already learns an instantaneous graph, we reuse the learned orientations of the model, and only relearn the edge existence parameters, γ , for potential pruning. In general, we found that the graphs predicted by iCITRIS have a few redundant edges between ancestors and descendants, which occur due to correlations in the early training iterations, and can easily be removed in this post-processing step.

As an additional metric to jointly evaluate the disentanglement of the causal variables and the learned causal graph, we use the learned causal graph and distributions by ENCO to sample new data point under novel interventional settings. For each data point in the test dataset, we use the trained model to sample the latents in the next time step, and map them back to the true causal variable space. This mapping is done by a small neural network, trained on the latents of the training dataset. To evaluate how well these samples match the interventional distributions of the true causal model, we train a small discriminator network which tries to distinguish between the true data points in the test set, and the newly generated ones from our model. Only a model that has disentangled the causal variables, *and* learned the correct causal graph, can perform well on this metric. We show the results for this metric on the Voronoi benchmark and the Instantaneous Temporal Causal3DIdent dataset in Appendix F.

Table 4: Summary of the hyperparameters for all models evaluated on the Voronoi benchmark, Instantaneous Temporal Causal3DIdent dataset, and the Causal Pinball dataset. For all methods, we performed a hyperparameter search over the individual, most crucial hyperparameters (e.g. KLD factor in iVAE). The smaller networks in the latter two datasets for the iVAE architectures were chosen because they require training the full encoder, decoder, and NF at the same time, and larger networks did not show any noticeable improvements. The graph learning warmup in iCITRIS is equal for all datasets, although deviations to e.g. 5k, 15k or 20k often work equally well. Further, the weighting parameters of target classifier and mutual information estimator for iCITRIS, such that, for instance, equally good results were achieved with smaller (5) or higher (20) weights on the Voronoi benchmark. For the graph sparsity regularizer, we used the same value for all graph structures of the same size.

Voronoi benchmark					
Hyperparameter	iCITRIS-ENCO	iCITRIS-NOTEARS	CITRIS	iVAE	iVAE-AR
Learning rate		— 1e-3 —			
Learning rate warmup		— 100 steps —			
Optimizer		— Adam (Kingma and Ba, 2015) —			
Batch size		— 512 —			
Number of epochs		— 400 —			
KLD Factor (β)		— 10 —			
Num latents		— 2x number of causal variables —			
Model variant		— VAE with NF prior —			
Encoder		— 5 layer CNN + 2 linear layers —			
NF-based prior	— 4 layer, autoregressive affine coupling (Kingma et al., 2016) —				
Prior dependencies		— Independent Gaussians —			Autoregressive
Decoder		— 5 layer (deconv-)CNN + 2 linear layers —			
Hidden dimensionality		— 32 —			
Activation function		— Swish (Ramachandran et al., 2017) —			
Target classifier weight		— 10 —		n.a.	n.a.
MI weight		— 10 —	n.a.	n.a.	n.a.
Graph learning warmup		— 10k —	n.a.	n.a.	n.a.
Graph sparsity reg.	0.02 (K=4,6) / 0.004 (K=9)	0.002 (K=4,6) / 0.0004 (K=9)	n.a.	n.a.	n.a.

Instantaneous Temporal Causal3DIdent dataset					
Hyperparameter	iCITRIS-ENCO	iCITRIS-NOTEARS	CITRIS	iVAE	iVAE-AR
Learning rate		— 1e-3 —			
Learning rate warmup		— 100 steps —			
Optimizer		— Adam (Kingma and Ba, 2015) —			
Batch size		— 512 —			
Number of epochs		— 500 —		— 250 —	
KLD Factor (β)		— 1 —			
Num latents		— 32 —			
Model variant		— AE + NF —		— VAE with NF prior —	
Encoder		— 10-layer CNN (AE) —		— 10-layer CNN (VAE) —	
Num flow layers		— 6 layers —		— 4 layers —	
Prior dependencies		— Autoregressive per z_{ψ_i} —		Independent	Autoregressive
Decoder		— 10-layer ResNet —		— 5-layer ResNet —	
Hidden dimensionality		— 64 (VAE/AE) / 32 (NF) —			
Activation function		— Swish (Ramachandran et al., 2017) —			
Target classifier weight		— 3 —	2	n.a.	n.a.
MI weight	2	1	n.a.	n.a.	n.a.
Graph learning warmup		— 10k —	n.a.	n.a.	n.a.
Graph sparsity reg.	0.02	0.0004	n.a.	n.a.	n.a.

Causal Pinball dataset					
Hyperparameter	iCITRIS-ENCO	iCITRIS-NOTEARS	CITRIS	iVAE	iVAE-AR
Learning rate		— 1e-3 —			
Learning rate warmup		— 100 steps —			
Optimizer		— Adam (Kingma and Ba, 2015) —			
Batch size		— 512 —			
Number of epochs		— 500 —		— 250 —	
KLD Factor (β)		— 1 —			
Num latents		— 24 —			
Model variant		— AE + NF —		— VAE with NF prior —	
Encoder		— 10-layer CNN (AE) —		— 10-layer CNN (VAE) —	
Num flow layers		— 6 layers —		— 4 layers —	
Prior dependencies		— Autoregressive per z_{ψ_i} —		Independent	Autoregressive
Decoder		— 10-layer ResNet —		— 5-layer ResNet —	
Hidden dimensionality		— 64 (VAE/AE) / 32 (NF) —			
Activation function		— Swish (Ramachandran et al., 2017) —			
Target classifier weight		— 4 —	2	n.a.	n.a.
MI weight	4	4	n.a.	n.a.	n.a.
Graph learning warmup		— 10k —	n.a.	n.a.	n.a.
Graph sparsity reg.	0.02	0.001	n.a.	n.a.	n.a.

Table 5: Experimental results of the large-scale study on the Voronoi benchmark with standard deviations over 5 seeds. We report the R^2 correlation (R^2 diag / R^2 sep), the SHD between the predicted and ground truth graph (instantaneous / temporal), and the accuracy of a discriminator distinguishing between true intervention samples and generated ones from the individual models (optimal 50%).

Model	#variables	Graph structure								
		R^2	Random SHD	Disc.	R^2	Chain SHD	Disc.	R^2	Full SHD	Disc.
iCITRIS-ENCO		0.99 / 0.00 (±0.00)/(±0.00)	0.00 / 0.00 (±0.00)/(±0.00)	55.71% (±1.52)	0.99 / 0.00 (±0.01)/(±0.00)	0.00 / 0.20 (±0.00)/(±0.45)	55.61% (±0.25)	0.97 / 0.00 (±0.01)/(±0.01)	0.00 / 0.60 (±0.00)/(±0.89)	56.25% (±1.56)
iCITRIS-NOTEARS		0.96 / 0.01 (±0.01)/(±0.00)	0.00 / 0.40 (±0.00)/(±0.55)	57.43% (±4.41)	0.89 / 0.08 (±0.14)/(±0.12)	1.40 / 1.60 (±1.67)/(±2.07)	65.28% (±16.51)	0.94 / 0.02 (±0.03)/(±0.03)	0.00 / 3.20 (±0.00)/(±2.39)	56.42% (±0.40)
CITRIS	4	0.86 / 0.09 (±0.09)/(±0.08)	1.00 / 2.60 (±1.22)/(±1.52)	59.10% (±3.47)	0.83 / 0.12 (±0.08)/(±0.08)	2.00 / 4.20 (±1.58)/(±2.17)	60.77% (±2.68)	0.73 / 0.17 (±0.12)/(±0.11)	2.80 / 5.80 (±0.84)/(±1.64)	63.06% (±2.95)
iVAE		0.74 / 0.20 (±0.18)/(±0.18)	1.00 / 4.20 (±0.71)/(±3.63)	65.41% (±8.14)	0.75 / 0.19 (±0.14)/(±0.16)	2.80 / 6.40 (±1.92)/(±1.52)	66.28% (±5.97)	0.60 / 0.24 (±0.20)/(±0.13)	3.60 / 6.80 (±1.34)/(±1.79)	68.62% (±6.84)
iVAE-AR		0.84 / 0.21 (±0.15)/(±0.18)	1.80 / 3.00 (±1.64)/(±2.35)	69.85% (±6.78)	0.92 / 0.17 (±0.04)/(±0.09)	3.20 / 2.40 (±1.92)/(±1.67)	70.76% (±5.06)	0.86 / 0.32 (±0.07)/(±0.12)	4.60 / 3.60 (±1.14)/(±1.95)	77.60% (±12.68)
iCITRIS-ENCO		0.97 / 0.00 (±0.01)/(±0.00)	0.20 / 1.00 (±0.45)/(±1.22)	59.86% (±3.17)	0.98 / 0.00 (±0.00)/(±0.00)	0.00 / 0.20 (±0.00)/(±0.45)	59.31% (±1.84)	0.93 / 0.01 (±0.03)/(±0.01)	0.80 / 4.20 (±1.10)/(±4.38)	60.67% (±2.57)
iCITRIS-NOTEARS		0.95 / 0.01 (±0.03)/(±0.01)	0.80 / 3.40 (±1.30)/(±3.51)	61.48% (±3.93)	0.96 / 0.02 (±0.03)/(±0.03)	0.80 / 1.00 (±1.30)/(±2.24)	65.17% (±12.64)	0.81 / 0.07 (±0.14)/(±0.07)	4.75 / 7.75 (±5.91)/(±4.57)	73.34% (±13.32)
CITRIS	6	0.80 / 0.13 (±0.04)/(±0.03)	5.00 / 11.20 (±3.54)/(±2.59)	65.61% (±2.48)	0.80 / 0.15 (±0.05)/(±0.05)	2.80 / 9.80 (±2.05)/(±2.77)	65.54% (±2.82)	0.70 / 0.14 (±0.03)/(±0.03)	11.20 / 12.40 (±2.59)/(±2.70)	67.63% (±1.18)
iVAE		0.70 / 0.22 (±0.08)/(±0.08)	5.40 / 14.60 (±3.36)/(±4.10)	69.99% (±3.11)	0.70 / 0.23 (±0.04)/(±0.04)	3.40 / 13.20 (±1.14)/(±3.19)	69.44% (±2.76)	0.61 / 0.18 (±0.08)/(±0.04)	12.00 / 17.20 (±1.87)/(±2.59)	70.14% (±3.01)
iVAE-AR		0.77 / 0.24 (±0.12)/(±0.11)	8.20 / 9.20 (±1.30)/(±3.49)	79.28% (±2.87)	0.84 / 0.23 (±0.08)/(±0.11)	4.60 / 8.20 (±0.89)/(±2.86)	80.84% (±11.49)	0.75 / 0.24 (±0.09)/(±0.08)	12.60 / 9.00 (±0.55)/(±4.96)	83.75% (±9.15)
iCITRIS-ENCO		0.96 / 0.00 (±0.01)/(±0.00)	0.20 / 1.20 (±0.45)/(±1.10)	63.29% (±0.99)	0.97 / 0.00 (±0.00)/(±0.00)	0.00 / 0.00 (±0.00)/(±0.00)	62.91% (±1.17)	0.89 / 0.02 (±0.03)/(±0.01)	1.20 / 9.60 (±2.17)/(±5.86)	65.70% (±1.32)
iCITRIS-NOTEARS		0.88 / 0.05 (±0.06)/(±0.04)	1.40 / 2.40 (±2.61)/(±5.37)	64.92% (±3.86)	0.93 / 0.04 (±0.03)/(±0.02)	0.40 / 0.20 (±0.89)/(±0.45)	62.52% (±0.86)	0.74 / 0.09 (±0.05)/(±0.02)	14.50 / 9.00 (±0.71)/(±0.00)	70.71% (±2.49)
CITRIS	9	0.71 / 0.17 (±0.10)/(±0.08)	14.00 / 18.40 (±4.47)/(±5.90)	70.79% (±1.26)	0.84 / 0.10 (±0.03)/(±0.02)	3.00 / 13.00 (±1.22)/(±1.58)	67.44% (±1.33)	0.68 / 0.11 (±0.03)/(±0.02)	32.40 / 22.40 (±1.52)/(±2.41)	73.62% (±1.07)
iVAE		0.65 / 0.22 (±0.09)/(±0.07)	13.60 / 24.00 (±2.88)/(±3.81)	71.78% (±1.27)	0.71 / 0.21 (±0.04)/(±0.03)	4.80 / 27.60 (±1.48)/(±5.27)	71.86% (±3.20)	0.61 / 0.15 (±0.06)/(±0.05)	32.40 / 29.20 (±1.14)/(±5.72)	74.22% (±1.85)
iVAE-AR		0.69 / 0.22 (±0.10)/(±0.03)	17.60 / 21.00 (±2.97)/(±7.28)	90.25% (±8.73)	0.80 / 0.18 (±0.12)/(±0.11)	7.80 / 16.00 (±3.56)/(±9.25)	79.12% (±2.51)	0.70 / 0.21 (±0.05)/(±0.03)	34.00 / 16.40 (±1.73)/(±4.83)	85.85% (±0.40)

F Additional experimental results

In this section, we list the detailed results of the experiments in Section 5, including the standard deviations over multiple seeds. We further provide results on the metric for predicting intervention outcomes, as described in Appendix E.3. Moreover, we present ablation studies on the Voronoi benchmark to further investigate the limitations of iCITRIS. Finally, in Appendix F.2, we include a visualization of the predicted graph by all models on the Instantaneous Temporal Causal3DIdent dataset.

F.1 Voronoi benchmark

The full experimental results for the Voronoi benchmark can be found in Table 5. Compared to the results in Figure 2, we also show the results of the discriminator that is trained on newly generated samples from the models. It is apparent that a crucial factor for simulating the true intervention distributions is to have low entanglement across other factors (R^2 sep). Both iVAE and especially iVAE-AR have a strong entanglement between factors, and show a significant gap between the true distribution and their modeled ones. For instance, on the random graphs of size 9, 90% of the samples can be correctly classified from iVAE-AR, indicating that the distributions do not overlap much. In comparison, iCITRIS achieves close-to optimal scores on the small graphs with 55% accuracy only. Note that 50% is already random performance, *i.e.* the optimum that could be achieved. Still, with larger graphs, we see that the performance also goes down for iCITRIS, although it still outperforms all baselines.

Furthermore, to show the specific failure types of the different models on graph prediction, we additionally list the recall and precision of the graph prediction (instantaneous - Table 6, temporal - Table 7). A high recall (max 1.00) reflects that the models are able to recover all edges, while a high precision (max 1.00) shows that the model do not overpredict false positive edges. One key characteristic on all models is that they tend to have a higher recall than precision for the temporal graph. In other words, many mistakes are due to predicting too many edges, which easily occurs

Table 6: Experimental results of the large-scale study on the Voronoi dataset for predicting the **instantaneous** graph, including the recall and precision to highlight false negative and positive predictions.

Model	#variables	Graph structure						Full		
		SHD	Random recall	precision	SHD	Chain recall	precision	SHD	recall	precision
iCITRIS-ENCO	4	0.00	1.00	1.00	0.00	1.00	1.00	0.00	1.00	1.00
iCITRIS-NOTEARS		0.00	1.00	1.00	1.40	0.73	0.80	0.00	1.00	1.00
CITRIS		1.00	0.60	0.55	2.00	0.73	0.62	2.80	0.53	0.90
iVAE		1.00	0.57	0.75	2.80	0.47	0.38	3.60	0.40	0.95
iVAE-AR		1.80	0.33	0.40	3.20	0.40	0.58	4.60	0.23	0.42
iCITRIS-ENCO	6	0.20	0.98	1.00	0.00	1.00	1.00	0.80	0.95	1.00
iCITRIS-NOTEARS		0.80	0.92	1.00	0.80	0.92	0.93	4.75	0.68	1.00
CITRIS		5.00	0.48	0.70	2.80	0.64	0.80	11.20	0.25	0.95
iVAE		5.40	0.36	0.70	3.40	0.56	0.66	12.00	0.20	0.85
iVAE-AR		8.20	0.19	0.26	4.60	0.44	0.60	12.60	0.16	0.65
iCITRIS-ENCO	9	0.20	1.00	0.99	0.00	1.00	1.00	1.20	0.97	1.00
iCITRIS-NOTEARS		1.40	0.96	0.96	0.40	1.00	0.96	14.50	0.60	1.00
CITRIS		14.00	0.25	0.68	3.00	0.82	0.81	32.40	0.10	1.00
iVAE		13.60	0.27	0.68	4.80	0.55	0.66	32.40	0.10	0.96
iVAE-AR		17.60	0.13	0.30	7.80	0.33	0.55	34.00	0.06	0.35

Table 7: Experimental results of the large-scale study on the Voronoi dataset for predicting the **temporal** graph, including the recall and precision to highlight false negative and positive predictions.

Model	#variables	Graph structure						Full		
		SHD	Random recall	precision	SHD	Chain recall	precision	SHD	recall	precision
iCITRIS-ENCO	4	0.00	1.00	1.00	0.20	1.00	0.97	0.60	1.00	0.92
iCITRIS-NOTEARS		0.40	1.00	0.94	1.60	0.93	0.81	3.20	1.00	0.68
CITRIS		2.60	1.00	0.70	4.20	1.00	0.60	5.80	1.00	0.51
iVAE		4.20	0.87	0.63	6.40	0.85	0.48	6.80	0.63	0.39
iVAE-AR		3.00	0.89	0.69	2.40	1.00	0.73	3.60	1.00	0.64
iCITRIS-ENCO	6	1.00	1.00	0.92	0.20	1.00	0.98	4.20	0.98	0.75
iCITRIS-NOTEARS		3.40	1.00	0.79	1.00	1.00	0.93	7.75	1.00	0.59
CITRIS		11.20	0.94	0.50	9.80	0.92	0.52	12.40	0.98	0.45
iVAE		14.60	0.79	0.42	13.20	0.91	0.44	17.20	0.87	0.36
iVAE-AR		9.20	0.85	0.55	8.20	0.98	0.56	9.00	0.90	0.54
iCITRIS-ENCO	9	1.20	1.00	0.94	0.00	1.00	1.00	9.60	1.00	0.71
iCITRIS-NOTEARS		2.40	1.00	0.92	0.20	1.00	0.99	9.00	0.95	0.72
CITRIS		18.40	0.84	0.55	13.00	1.00	0.62	22.40	0.92	0.48
iVAE		24.00	0.82	0.48	27.60	0.99	0.44	29.20	0.86	0.41
iVAE-AR		21.00	0.89	0.51	16.00	0.85	0.60	16.40	0.91	0.57

when causal variables are entangled. However, on the instantaneous graphs, we clearly see that the baselines, CITRIS and iVAE, predict a sparse graph by having a low recall. This also underlines that the false positive edges in the temporal graph cannot be simply removed by increasing the sparsity regularizer in the causal discovery method, since otherwise, even more edges would be lost in the

Table 8: Results of three ablation studies on the Voronoi benchmark, performed on the random graph with 6 variables. **Left (Intervention noise)**: We introduce noise on the intervention targets by introducing 10% false positive cases in the intervention targets, *i.e.* $I_i^t = 1$ although C_i is sampled from the observation distribution. iCITRIS-ENCO performs almost as well as before. **Middle (No instantaneous)**: We apply all methods on graphs with an empty instantaneous graph. iCITRIS-ENCO obtains almost perfect disentanglement along with CITRIS and iVAE, showing that iCITRIS can be used as a replacement of them under perfect interventions. **Right (No temporal)**: The most difficult setup is when the variables have purely instantaneous relations and samples between time steps are independent. In this case, no method can disentangle the variables well, showing that different optimization strategies than iCITRIS are needed in this setting.

Model	Ablation study					
	Intervention noise		No instantaneous		No temporal	
	R^2	SHD	R^2	SHD	R^2	SHD
iCITRIS-ENCO	0.96 / 0.00 (±0.01)/(±0.00)	0.20 / 4.00 (±0.45)/(±1.87)	0.99 / 0.00 (±0.00)/(±0.00)	0.00 / 0.00 (±0.00)/(±0.00)	0.55 / 0.21 (±0.08)/(±0.06)	6.80 / 0.00 (±2.39)/(±0.00)
CITRIS	0.78 / 0.14 (±0.09)/(±0.09)	5.00 / 10.60 (±4.58)/(±4.51)	0.99 / 0.00 (±0.00)/(±0.00)	0.00 / 0.00 (±0.00)/(±0.00)	0.54 / 0.21 (±0.06)/(±0.06)	6.80 / 0.00 (±2.39)/(±0.00)
iVAE	0.69 / 0.22 (±0.10)/(±0.11)	5.40 / 15.00 (±3.36)/(±3.39)	0.99 / 0.00 (±0.00)/(±0.00)	0.00 / 0.00 (±0.00)/(±0.00)	0.49 / 0.20 (±0.05)/(±0.02)	7.00 / 0.00 (±2.24)/(±0.00)
iVAE-AR	0.84 / 0.22 (±0.10)/(±0.06)	7.40 / 8.60 (±2.07)/(±3.44)	0.79 / 0.23 (±0.13)/(±0.06)	2.80 / 9.00 (±0.45)/(±4.42)	0.54 / 0.28 (±0.05)/(±0.02)	7.80 / 0.00 (±3.27)/(±0.00)

instantaneous graph. iVAE-AR, on the other hand, has a low precision *and* recall on the instantaneous graphs; showcasing that it predicts a very different graph with anticausal edges. Meanwhile, only iCITRIS-ENCO obtains a higher recall and precision across the different graph structures and sizes.

Next, we will look at additional ablation studies that investigate the applications and limitations of iCITRIS.

F.1.1 Ablation 1: Noisy intervention targets

In the first ablation study, we focus on the dependency of iCITRIS on accurate intervention targets. In practice, performing perfect interventions is a difficult task, and is prone to noise. While we can easily observe whether we pushed a button or did external actions to influence a dynamical system, we do not know for sure whether the intervention succeeded or not. This corresponds to a case where the intervention targets, I^t , are noisy and tend to have false positives, *i.e.* $I_i^t = 1$ although the intervention did not succeed. How sensitive is iCITRIS to such noise?

To investigate this question, we repeat the experiments of the Voronoi benchmark on the random graphs of size 6, but simulate that in 10% of the cases when I_i^t , we actually do not intervene on C_i and instead sample the value from its observational distribution. The results are summarized in Table 8 (left two columns), and clearly show that iCITRIS can yet work well in this setting. The variables are almost as well as before disentangled as before. The additional temporal variables are partially also because of noisy interventions in the post-processing causal discovery setting.

F.1.2 Ablation 2: Empty instantaneous graph

The main aspect of iCITRIS in contrast to the baselines is that supports instantaneous effects. However, in practice, we might not know whether instantaneous effects are in the data or not. Thus, this ablation study investigates, whether iCITRIS can yet be used as a replacement of the baselines like CITRIS, when perfect interventions are provided. For this, we repeat the experiments of the Voronoi benchmark on causal models with an empty instantaneous of size 6. As the results in Table 8 show, iCITRIS, CITRIS, and iVAE all are able to identify the causal variables and the graph. This show that iCITRIS can indeed be used as a replacement of CITRIS and iVAE, even in the setting that the variables are independent, conditioned on the previous time step.

Table 9: Experimental results on the Instantaneous Temporal Causal3D dataset, with standard deviations across three seeds.

Model	R^2	Spearman	Triplets	SHD (Instant)	SHD (Temp)	Disc. Acc.
iCITRIS-ENCO	0.96 / 0.05 (±0.00) / (±0.00)	0.96 / 0.10 (±0.00) / (±0.00)	0.09 (±0.00)	1.33 (±1.15)	5.00 (±1.73)	55.41% (±0.87%)
iCITRIS-NOTEARS	0.95 / 0.09 (±0.00) / (±0.01)	0.95 / 0.14 (±0.01) / (±0.01)	0.14 (±0.00)	4.00 (±1.00)	5.00 (±1.73)	61.05% (±4.43%)
CITRIS	0.92 / 0.19 (±0.01) / (±0.02)	0.90 / 0.22 (±0.01) / (±0.01)	0.19 (±0.01)	4.67 (±0.58)	10.00 (±2.00)	67.51% (±5.90%)
iVAE	0.82 / 0.20 (±0.02) / (±0.01)	0.80 / 0.22 (±0.02) / (±0.01)	0.27 (±0.01)	6.67 (±2.52)	15.33 (±1.53)	86.87% (±2.71%)
iVAE-AR	0.79 / 0.29 (±0.01) / (±0.03)	0.78 / 0.33 (±0.02) / (±0.00)	0.27 (±0.01)	11.00 (±1.00)	12.67 (±1.53)	87.07% (±0.90%)

F.1.3 Ablation 3: Empty temporal graph

As a final ablation study, we consider the most difficult setup, namely having no temporal relations at all. In this case, all relations between causal variables are purely instantaneous, and we cannot use any information of the previous time step, *i.e.* z^t , as an initial guidance for disentangling the variables. Once more, we repeat the experiments of the Voronoi benchmark on the random graphs of size 6, but with an empty instantaneous graph, and summarize the results in Table 8 (right columns). Due to the difficulty of the task, none of the methods was able to identify the causal variables. Since the probabilities of the edges in iCITRIS are initially around 0.5, the model focuses on finding K independent factors of variations instead of the causal variables. The balance that is crucial for the temporal setup is that the knowledge of the interventions and previous time step is more important than the instantaneous effects for some variables, which, in this case, does not hold. Hence, to overcome this problem, different optimization strategies than the ones discussed in Section 4.2 are needed. Interestingly, even the autoregressive iVAE fails at going beyond finding K independent factors, underlining the difficulty of the task.

F.2 Instantaneous Temporal Causal3DIdent experiments

The full experimental results, including standard deviations across three seeds for all models, are shown in Table 9. Next to the correlation and graph prediction metrics, we also list the results of the triplet evaluation following Lippe et al. (2022b), and the discriminator accuracy of distinguishing between true and fake interventional samples. The triplet distance measures how well we can perform combinations of causal factors in latent space without causing correlations among different factors. For instance, if we combine the causal factors from image 1 with the object hue of image 2, how close is the decoded image to those true factors? The results show that the small differences in entanglement between iCITRIS-ENCO and iCITRIS-NOTEARS lead to considerable difference for generating new combinations of causal factors, highlighting the importance of strong disentanglement between causal factors. Similarly, the discriminator accuracy shows that iCITRIS-ENCO can accurately model the distribution of the true causal model, while clear differences to the VAE-based baseline, iVAE and iVAE-AR, are visible.

To get an intuition on what graphs the different models identify, we have visualized on example of each model in Figure 17. In general, we see that iCITRIS-ENCO misses only one edge which is sparse anyway, since hue_b affects hue_o only for two shapes. Similarly to the results of Lippe et al. (2022b), we find that the object shape is a false positive parent of the rotation of the object. For CITRIS, we see that it starts to predict incorrect orientations due to correlations among factors. Finally, iVAE and iVAE-AR predict graphs that have little in common with the ground truth one.

F.3 Causal Pinball

Finally, the full experimental results for the Causal Pinball environment can be found in Table 10. Besides the correlation and graph metrics, we again report the triplet evaluation, which shows once more that iCITRIS and CITRIS both work well here.

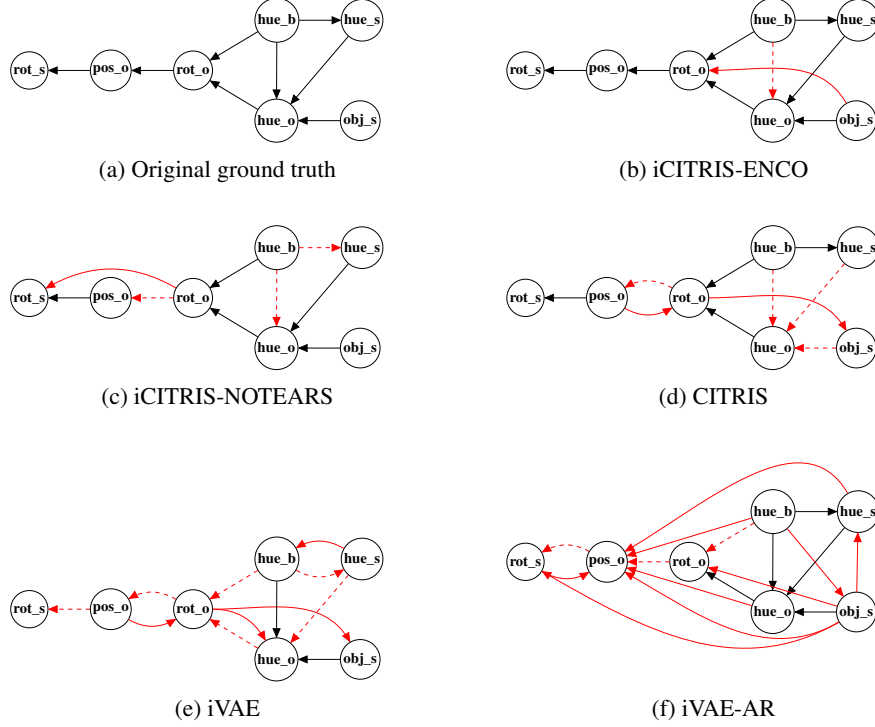


Figure 17: Learned instantaneous graphs in the Instantaneous Temporal Causal3DIIdent dataset for all five models for a single seed. Red arrows indicate false positive edges, and dashed red arrows false negatives. (a) The ground truth of the dataset. (b) iCITRIS-ENCO achieves for one score a perfect recovery of the graph, and for the other two graphs, we miss one edge to hue_o since hue_b only affects it for certain object shapes, and have an additional from the object shape to the rotation due to the complexity of the problem. (c) iCITRIS-NOTEARS had more false positive and negative edges than iCITRIS-ENCO. However, all orientations were correct. (d) CITRIS had in general a sparser graph than the true graph, but in contrast to iCITRIS, also obtained wrong orientations several times (e.g. between pos_o and rot_o). (e) The iVAE obtains very different graphs from the ground truth, with many incorrectly edges. (f) Due to the autoregressive prior in iVAE-AR, we observed a significant amount of false positive edges, with occasional incorrect orientation as well.

Table 10: Experimental results on the Causal Pinball dataset over three seeds.

Model	R^2	Spearman	Triplets	SHD (Instant)	SHD (Temp)
iCITRIS-ENCO	0.98 / 0.04 (±0.00) / (±0.01)	0.99 / 0.17 (±0.00) / (±0.03)	0.02 (±0.00)	0.67 (±0.58)	3.67 (±1.15)
iCITRIS-NOTEARS	0.98 / 0.06 (±0.00) / (±0.04)	0.99 / 0.19 (±0.00) / (±0.06)	0.02 (±0.00)	2.33 (±0.58)	3.67 (±0.58)
CITRIS	0.98 / 0.04 (±0.01) / (±0.01)	0.99 / 0.18 (±0.00) / (±0.02)	0.02 (±0.00)	2.67 (±1.53)	4.00 (±1.00)
iVAE	0.55 / 0.04 (±0.08) / (±0.03)	0.58 / 0.14 (±0.09) / (±0.06)	0.55 (±0.06)	2.33 (±0.58)	4.33 (±1.15)
iVAE-AR	0.53 / 0.15 (±0.08) / (±0.09)	0.55 / 0.30 (±0.09) / (±0.08)	0.56 (±0.06)	4.33 (±1.53)	6.33 (±1.53)

Further, we visualize the predicted causal graphs of the different methods in Figure 18. In general, we found that the most difficult relations are between the paddles and the ball, in particular their orientation. This is due to the deterministic relations between the two factors, such that if the ball has been hit by the paddle, we can already predict it just from the ball position. Further, in many states, the ball and paddle do not affect each other, such that a state where the paddle would have hit the ball, but the ball was intervened upon in the same time step, is extremely rare. Overall, all models suffered from this problem, but iCITRIS showed to handle it.

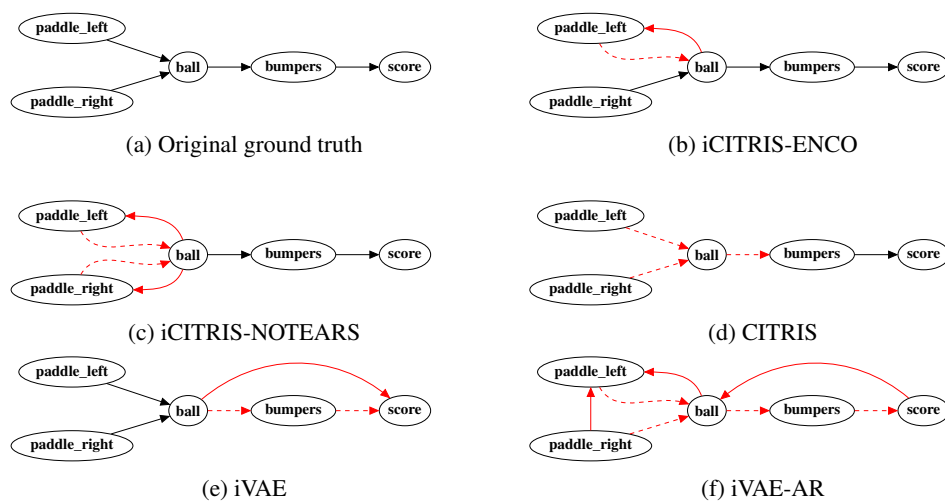


Figure 18: Learned instantaneous graphs in the Causal Pinball dataset for all five models for a single seed. Red arrows indicate false positive edges, and dashed red arrows false negatives. (a) The ground truth of the dataset. (b) iCITRIS-ENCO recovered the graph for one seed perfectly, and for the other two seeds, incorrectly oriented an edge between the ball and paddles. (c) iCITRIS-NOTEARS commonly has some incorrect orientations between the paddles and the ball. (d) CITRIS, similar to other experiments, tends to have a sparser instantaneous graph. (e) iVAE has a sparser graph, similar to CITRIS, but with additional false positive edges. (f) iVAE-AR predicts a causal graph that has no edge in common with the true graph.